THE SCATTERING PROCESS OF CYLINDRICAL WAVES BY A CONVEX HYPERBOLIC REFLECTOR

SÜLEYMAN BURAK ÇELİK

SEPTEMBER 2015

THE SCATTERING PROCESS OF CYLINDRICAL WAVES BY A CONVEX HYPERBOLIC REFLECTOR

A THESIS SUBMITTED TO
THE GRADUATE SCHOOL OF NATURAL AND APPLIED SCIENCES OF
ÇANKAYA UNIVERSITY

BY
SÜLEYMAN BURAK ÇELİK

IN PARTIAL FULFILLMENT OF THE REQUIREMENTS FOR THE DEGREE OF
MASTER OF SCIENCE
IN
THE DEPARTMENT OF
ELECTRONIC AND COMMUNICATION ENGINEERING

SEPTEMBER 2015

Title of the Thesis : **The Scattering Process of Cylindrical Waves by A Convex Hyperbolic Reflector.**

Submitted by **Süleyman Burak ÇELİK**

Approval of the Graduate School of Natural and Applied Sciences, Çankaya University.

Prof. Dr. Halil Tanyer EYYUBOĞLU
Director

I certify that this thesis satisfies all the requirements as a thesis for the degree of Master of Science.

Prof. Dr. Halil Tanyer EYYUBOĞLU
Head of Department

This is to certify that we have read this thesis and that in our opinion it is fully adequate, in scope and quality, as a thesis for the degree of Master of Science.

Prof. Dr. Yusuf Ziya UMUL
Supervisor

Examination Date: 01.09.2015

Examining Committee Members

Assoc. Prof. Dr. Nursel AKÇAM	(Gazi Univ.)	
Prof. Dr. Yusuf Ziya UMUL	(Çankaya Univ.)	
Asst. Prof. Dr. Hüsnü Deniz BAŞDEMİR	(Çankaya Univ.)	

STATEMENT OF NON-PLAGIARISM PAGE

I hereby declare that all information in this document has been obtained and presented in accordance with academic rules and ethical conduct. I also declare that, as required by these rules and conduct, I have fully cited and referenced all material and results that are not original to this work.

Name, Last Name : Süleyman Burak ÇELİK

Signature : SBÇ

Date : 01.09.2015

ABSTRACT

THE SCATTERING PROCESS OF CYLINDRICAL WAVES BY A CONVEX HYPERBOLIC REFLECTOR

ÇELİK, Süleyman Burak
M.Sc., Department of Electronic and Communication
Supervisor: Prof. Dr. Yusuf Ziya UMUL

September 2015, 69 pages

In this thesis, the scattered fields by a perfectly conducting convex hyperbolic reflector were investigated by using the methods of modified theory of physical optics and physical optics. Furthermore, the geometrical optics and edge diffracted fields were evaluated by the stationary phase method and the edge point technique, respectively. The uniform diffracted field expressions were obtained by the method of the uniform theory of diffraction. Moreover, the results of modified theory of physical optics and physical optics were plotted and compared numerically. The results of geometrical optics and uniform diffracted fields were also plotted and analyzed numerically.

Keywords: Convex Hyperbolic Reflector, Modified Theory of Physical Optics, Physical Optics, Reflected and Transmitted Fields, Edge Diffraction, Uniform Diffracted Fields.

ÖZ

SİLİNDİRİK DALGALARIN DISBÜKEY HİPERBOLİK BİR YANSITICIDAN SAÇILMASI

ÇELİK, Süleyman Burak
Yüksek Lisans, Elektronik ve Haberleşme Mühendisliği Anabilim Dalı
Tez Yöneticisi: Prof. Dr. Yusuf Ziya UMUL

Eylül 2015, 69 sayfa

Bu tezde, mükemmel iletken dışbükey hiperbolik bir yansıtıcıdan saçılan alanlar, fiziksel optiğin değiştirilmiş teorisi ve fiziksel optik teorisi yöntemleri kullanılarak incelenmiştir. Bununla birlikte, geometrik optik ve köşe kırınım alanları durağan faz yöntemi ve köşe noktası tekniği ile hesaplanmıştır. Düzgün kırınımlı alan ifadeleri kırınımın düzgün teorisi yöntemi ile elde edilmiştir. Dahası, fiziksel optiğin değiştirilmiş teorisi ile fiziksel optiğin sonuçları çizdirilmiş ve sayısal olarak karşılaştırılmıştır. Geometrik optik ve düzgün kırınım alanlarının sonuçları da bununla birlikte çizdirilmiş ve sayısal olarak analiz edilmiştir.

Anahtar Kelimeler: Dışbükey Hiperbolik Yansıtıcı, Fiziksel Optiğin Değiştirilmiş Teorisi, Fiziksel Optik, Yansıyan ve Taşınan Alanlar, Köşe Kırınımı, Düzgün Kırınımlı Alanlar.

ACKNOWLEDGEMENTS

I would like to express my sincere gratitude to Prof. Dr. Yusuf Ziya UMUL for his supervision, special guidance, suggestions, and encouragement during the development of this thesis.

It is a pleasure to express my special thanks to my family for their valuable support.

TABLE OF CONTENTS

LIST OF FIGURES

FIGURES

LIST OF ABBREVIATIONS

PEC	Perfectly Electric Conductor
PO	Physical Optics
MTPO	Modified Theory of Physical Optics
UTD	Uniform Theory of Diffraction
UAT	Uniform Asymptotic Theory of Diffraction
RCS	Radar Cross Section
HF	High Frequency
GTD	Geometrical Theory of Diffraction
PTD	Physical Theory of Diffraction
GO	Geometrical Optics

CHAPTER 1

INTRODUCTION

1.1 Objectives

In this thesis, the scattered fields are investigated through a convex hyperbolic reflector using methods of modified theory of physical optics and physical optics. The geometrical optics and edge diffracted fields are evaluated by the stationary phase method and the edge point technique. Besides, the uniform diffracted field expressions are obtained using the method of uniform theory of diffraction. The results of modified theory of physical optics and the physical optics are plotted and compared numerically. Moreover, the results of geometrical optics and uniform diffracted fields are also plotted and analyzed numerically. The reflector is used as a Perfectly Electric Conductor (PEC) surface for these purposes.

1.2 Background

The reflector antenna is conceptually one of the simplest antenna prototypes which mostly consist of a primary radiator or feed to distribute electromagnetic energy and a curved reflecting surface to collimate this energy over a larger aperture [1]. These types of antennas can be used for some applications such as radar, radioastronomy and microwave communication systems. A large variety of such antennas exist out of the simple parabolic reflector to Cassegrain and dual reflectors. Reflector antennas have been primarily used in several types of communication systems such as satellite communications and networks, deep-space exploration and electronics defense over the last years [2]. There are several types of reflectors that can be mainly named as parabolic reflector, hyperbolic reflector and elliptical reflector. These reflectors are used in dual-reflector systems which consist of one main reflector and one

subreflector. While the parabolic reflector is used as the main reflector, the hyperbolic and elliptical reflectors are used as subreflectors. Whereas the combination of a parabolic reflector and an elliptical reflector is named as Gregorian system, the combination of a parabolic reflector and a hyperbolic reflector is named as Cassegrain system. The hyperbolic reflector is used in the Cassegrain system [3]. Cassegrain systems are originally used in optical telescopes and widely used in the radio frequency field since they have numerous mechanical and electrical advantages [4]. In this thesis, the hyperboloid part of the Cassegrain system is studied and the scattering process is investigated by some methods that are going to be introduced in the next chapter.

There are several studies conducted on the hyperbolic reflector. Especially, the Cassegrain system has been investigated by many researchers. Determination of the radiation pattern of a focus-fed offset hyperbolic reflector using the Uniform geometrical Theory of Diffraction (UTD) and the Uniform Asymptotic Theory of diffraction (UAT) was investigated by Şafak [5]. A large dual-reflector (Cassegrain) antenna system, typically used as a ground station antenna in the space communication link was researched by Farahat, Mittra, Carrio´n and Sanchez [6]. Elkamchowhi[1], Elkamchowhi[2], El-Khamy [7] conducted an analysis on cylindrical hyperbolic reflector through the Method of Moments. The monostatic Radar Cross Section (RCS) behavior of the parabolic and hyperbolic reflectors was investigated by ˇSkokic´, Martini and Maci [8]. Fomel and Kazinnik [9] suggested a new form of the stacking surface, derived from the analytical solution for reflection traveltime from a hyperbolic reflector. A transient analysis of a hyperbolic reflector antenna based on a mathematic continuation of surface curvatures of an ellipsoidal reflector was performed by Chou and Tuan [10]. A type of feed-reflector system for large Cassegrain antennas of radio astronomy and deep-space communication applications was investigated by Mousavi, Shafai, Veidt and Dewdney [11]. Xiao, Yang, Liu, Xu, Xiong [12] analyzed the loss of the secondary mirror of Cassegrain antenna via Gaussian theory. Due to severe energy loss caused by the secondary mirror of Cassegrain antenna, an optimum structure design of the transmitting energy of Cassegrain optical system was improved by Ma, Yang, Wang, Jiang, Yu, Huang and Ke [13]. By detailed analysis on Cassegrain optical antenna with inclined optical axis, the receiving antenna power and the curve of power attenuation for different deflection angles were obtained by Chen, Yang,

Wang[i], Wang[ii] and Huang [14]. Haeger and Lee compared shaped and nonshaped small Cassegrain Antennas [15]. A simple ray tracing based on the synthesis technique for designing a dual shaped hyperbolic reflector feed system was described by Hakli', Ala-Laurinaho', Koskinen', Saily', Lonnqvist', Mallat', Tuovinen and Raisanen' [16]. The design of a dichroic subreflector for a dual-frequency reflector antenna was defined by Agrawal and Imbriale [17]. Using the first order equations, Galindo, Imbriale and Mittra [18] conducted the synthesis of single and dual offset shaped reflector antennas. The formulation of the Physical Optics (PO) integral from a hyperbolic subreflector illuminated by a focal feeder was obtained by Pippi, Caruso, Sabbadini and Maci [19]. A configuration of dual reflector antenna for radar applications in X band was presented by Armogida, Pagana, Stringhetti and Volpi [20]. The case of hyperbolic defocus due to its analytic form was modeled by Tyo, Farr and Lawry [21]. The design of dichroic mirror for space applications was presented by Bozzi, Formaggi and Perregrini [22]. A shaping method for offset dual reflector antennas was presented by Kim and Lee [23]. Jiang, Li, Zhou and Luo developed high-precision reflector panels [24]. A novel two dimensional circular lens for beam steering applications using hyperbolic reflector was presented by Mirkamali and Laurin [25]. A type of two-dimensional circular lens with the hyperbolic reflector based on Gaussian optics was designed by Mirkamali, Laurin, Siaka and Deban [26].

1.3 Scheme of the Thesis

This thesis includes six chapters. These chapters are mainly based on the scattering process through a hyperbolic reflector using the methods of the modified theory of physical optics and the physical optics. The geometrical optics fields, the edge point diffraction and the uniform diffracted fields can be found in this study with all their numerical analysis.

Chapter 1 is the introduction part that gives the information about reflectors, the history of hyperbolic reflector and objectives of this thesis.

Chapter 2 offers information about the methods of physical optics and modified theory of physical optics.

The hyperbola geometry is studied in Chapter 3.

In Chapter 4, the scattering by the convex hyperbolic reflector is investigated based mainly on the method of the modified theory of physical optics. The geometrical optics and edge diffracted fields are obtained. The uniform diffracted field expressions are also evaluated in this chapter.

The results of all field expressions obtained in Chapter 4 are analyzed numerically in Chapter 5.

Chapter 6, which is the final chapter of this thesis includes the part conclusions.

CHAPTER 2

METHODS

2.1 Electromagnetic Scattering

The general total field expression can be written as

$$u_t = u_i + u_s \tag{2.1}$$

where u_i and u_s are the incident field and the scattered field, respectively. The aim is to obtain the scattered field. It can be obtained by solving the Helmholtz equation for simple geometries. If the geometry is not simple, the scattered field can be obtained using of High Frequency (HF) asymptotic techniques which can be divided into two basic categories being ray based techniques and current based techniques. The Geometrical Optics (GO) [27], GTD [28] and UTD [29] can be given as the examples for ray based techniques. The theory of PO [30], the physical theory of diffraction (PTD) [31] and the Modified Theory of Physical Optics (MTPO) [32] are the examples for current based techniques. The high frequency asymptotic condition is satisfied when $k\rho \gg 1$ where k is the wave number and ρ is the distance between the source and observation point.

This study mainly depends on MTPO since it gives more reliable solution than PO does owing to its axioms. However, PO is also taken into consideration in order to compare the results of MTPO and PO in the part of numerical analysis.

The time factor $\exp(j\omega t)$ is assumed and suppressed throughout this thesis where j is $\sqrt{-1}$, ω is the angular frequency and t is time.

2.2 Physical Optics (PO)

Physical optics which was firstly introduced by Macdonald in 1912 [30] is a current based technique that depends on the integration of the induced surface current density. The induced surface current density is defined on the illuminated side of the scattering object. The surface current density of the shadowed part of the object is defined as zero.

Since 1950s, PO has been extensively used in many areas. It is mainly used as a tool for the estimation of scattering by military vehicles such as tanks, airplanes, ships, spacecraft, weapons, missiles and in the design of microwave antennas [33].

Despite the fact that PO is an important approach to find the scattered fields, it has a problem to find exact edge diffracted fields [34]. The reason of the problem is based on the shadowed part of the object. In this part of the object, since its surface current density is accepted as zero, the wedge diffraction problem cannot exactly be solved by the PO approach. Some alternative ways have been developed in order to make a correction for this deficiency in PO. For instance, Ufimtsev introduced a way in the physical theory of diffraction [31]. Ufimtsev proposed the addition of a second current component, named as the non-uniform or fringe current so that the correct diffracted field expressions can be obtained [35]. James also suggested a correction factor multiplied by the PO diffraction field instead of summing [36]. However, they need some exact coefficients for some canonical problems. As a result, these alternative ways could not be the exact cure of PO. In order to correct this deficiency, the modified theory of physical optics (MTPO) was suggested by Umul in 2004 [32].

2.3 Modified Theory of Physical Optics (MTPO)

MTPO which was partly mentioned in previous topic is the theory fixing the deficiencies in PO. It can be obviously seen in Ref. [32] that MTPO integral gives the total field that agrees with the exact solution and it gives more reliable result than classical PO integral. Since MTPO is useful to obtain the exact fields for several surfaces, it was applied to several geometries such as parabolic impedance surface [37] and impedance half plane problem [38]. Umul has defined three axioms for this

method. First, the scatterer is taken into consideration with its aperture part. Second axiom is the reflection angle that is taken as a function of the scatterer surface and aperture part coordinates. Third one is a new unit vector that divides the angle between the reflected and incident rays into two equal parts.

In PO, only information can be obtained is about reflected and reflected diffracted fields. However, in MTPO, information can be obtained also about incident and incident diffracted fields since both the scattering object surface and the aperture part of the scatterer are considered together.

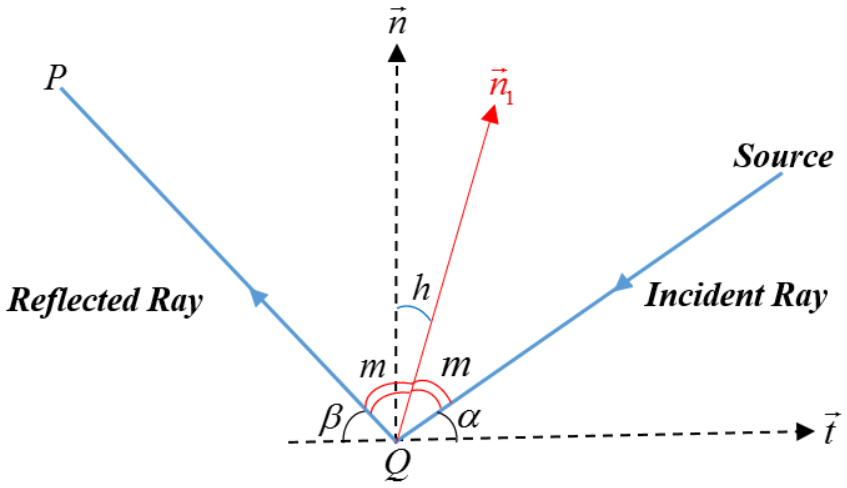

Figure 1 Reflection geometry at point Q of the scatterer

Figure 1 shows the reflection geometry at point Q where α and β are the angles of incidence and reflection, respectively. The incident and reflected rays can also be seen here. $\vec{n}$ and $\vec{t}$ are the normal and tangential vectors of the scatterer, respectively. $\vec{n}_1$ is the modified normal vector of the scatterer surface which can be expressed as

$$\vec{n}_1 = \cos(m+\alpha)\vec{t} + \sin(m+\alpha)\vec{n} \tag{2.2}$$

where m and h can be written as

$$m = \frac{\pi}{2} - \frac{\beta+\alpha}{2} \tag{2.3}$$

and

$$h = \frac{\alpha-\beta}{2} \tag{2.4}$$

according to the geometry in Fig. 1. Briefly, the other difference between PO and MTPO comes from writing the density of the surface currents. For a PEC scatterer, densities of surface currents of PO and MTPO can be defined as

$$\vec{J}_{PO} = 2\vec{n} \times \vec{H}_i \tag{2.5}$$

and

$$\vec{J}_{MTPO} = \vec{n}_1 \times \vec{H}_t \tag{2.6}$$

where $\vec{H}_i$ and $\vec{H}_t$ are the incident and total magnetic fields, respectively. It can be seen that the total field is considered as twice of the incident field for the surface current density of PO. However, the total field is considered with the modified normal vector in MTPO. The modified unit vector is used for both scatterer surface and aperture part. The detailed information about MTPO and its axioms can be obtained in Ref. [32].

In this thesis, the surface current density of the hyperbolic reflector will be written in terms of the modified theory of physical optics as in Eq. (2.6). In addition, Eq. (2.5) will also be considered in order to compare PO with MTPO numerically.

CHAPTER 3

EXACT EXPRESSION OF THE HYPERBOLA GEOMETRY

3.1 Hyperbola

With the purpose of evaluating the scattered fields from the hyperbola, its mathematical expression should first be determined on the coordinate system. A hyperbola has two pieces and two focal points. The pieces refer to the surfaces. In this study, one focal point and the convex part of surface are chosen. An electric line source is set on the focal point in order to illuminate the surface.

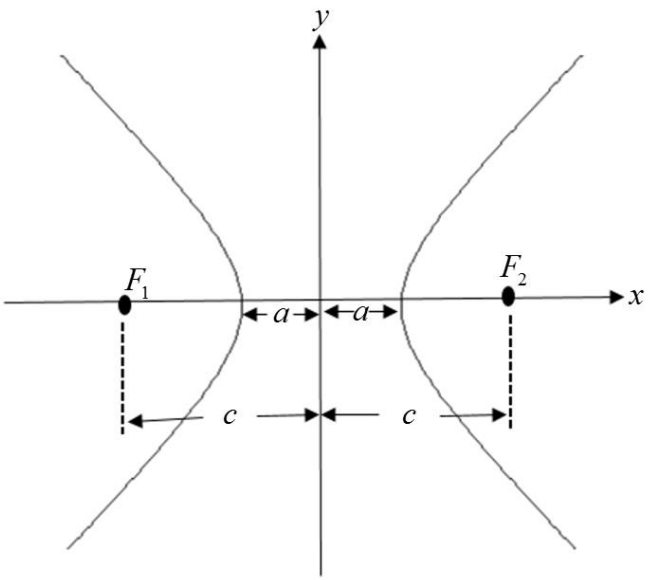

Figure 2 General notation of the hyperbola geometry on the coordinate system

Figure 2 shows the general notation of the hyperbola geometry on $x-y$ coordinate system where F_1 and F_2 are the focal points of the pieces of the hyperbola. a and c are the distance from the center to a piece of the hyperbola and the distance from the center to one focal point, respectively. The equation of the hyperbola can be written as

$$\frac{x^2}{a^2}-\frac{y^2}{b^2}=1 \tag{3.1}$$

where b is equal to $\sqrt{c^2-a^2}$.

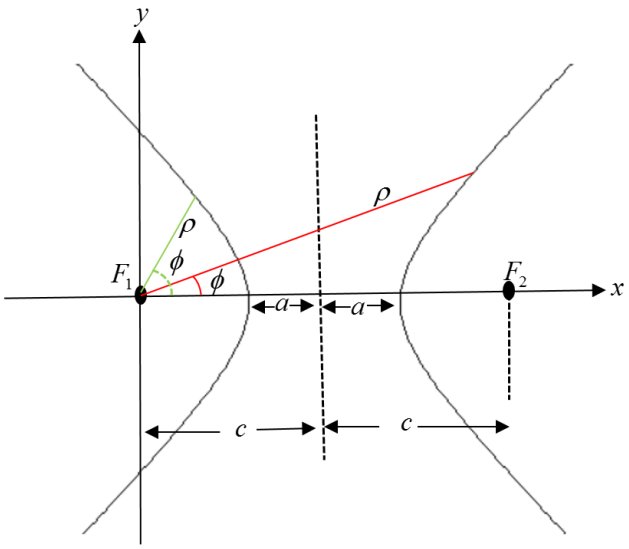

Figure 3 Shifted geometry of the hyperbola

Figure 3 shows the hyperbola geometry where the focal point F_1 was shifted to the center of the coordinate system in order to obtain ρ values which represent the paths from the center to the surfaces that travel on the surfaces when the angle ϕ changes. There can be seen two values of ρ in Fig. 3. One of them is related with one surface of the hyperbola, the other one is related to the other surface of the hyperbola. This means that one of the values of ρ travels on the left surface of the hyperbola and the other value of ρ travels on the right piece of the hyperbola. Since the convex part of the hyperbola is the right surface of the hyperbola, the value of ρ that travels on the right surface of the hyperbola will be determined as the exact ρ for this study. The value of ρ can be obtained by solving Eq. (3.1) in terms of cylindrical coordinates and it is used in MTPO integral.

3.2 Determination of the Exact ρ From the Hyperbola Geometry

When Eq. (3.1) is solved in terms of cylindrical coordinates, there will be two ρ values. According to Fig. 3, x can be written as

$$x = \rho\cos\phi - c \tag{3.2}$$

where $-c$ refers to the focal point F_1 that is brought to the center of the coordinate system by shifting to right as the distance c. The parameter y can be written as

$$y = \rho\sin\phi. \tag{3.3}$$

The variable c can also be defined as

$$c = ea \tag{3.4}$$

where e is the eccentricity which is dimensionless number and it is always greater than one. Eq. (3.1) can be rearranged as

$$b^2x^2 - a^2y^2 = a^2b^2. \tag{3.5}$$

Then, equivalents of x and y defined in Eq. (3.2) and Eq. (3.3), Eq. (3.5) using the cylindrical coordinate can be expressed as

$$b^2\left(\rho^2\cos^2\phi - 2ea\rho\cos\phi + e^2a^2\right) - a^2\rho^2\sin^2\phi = a^2b^2 \tag{3.6}$$

where b^2 can be obtained as

$$b^2 = (ea)^2 - a^2. \tag{3.7}$$

Finally, the parameter b can be obtained as

$$b = a\sqrt{e^2 - 1}. \tag{3.8}$$

By using Eq. (3.7), Eq. (3.6) can be redefined as

$$a^2\left(e^2-1\right)\left(\rho^2\cos^2\phi - 2ea\rho\cos\phi + e^2a^2\right) - a^2\rho^2\sin^2\phi = a^2a^2\left(e^2-1\right), \tag{3.9}$$

which can be expanded as

$$\begin{aligned} &e^2\rho^2\cos^2\phi - 2e^3a\rho\cos\phi + e^4a^2 - \rho^2\cos^2\phi + 2ea\rho\cos\phi - e^2a^2 \\ &= e^2a^2 - a^2 + \rho^2\sin^2\phi. \end{aligned} \tag{3.10}$$

Since the aim is to find the variable ρ, Eq. (3.10) can be rearranged in terms of the variable ρ. The quadratic equation for ρ can be expressed as

$$\rho^2\left(e^2\cos^2\phi - 1\right) + \rho\left(2ae\cos\phi - 2e^3a\cos\phi\right) + e^4a^2 - 2a^2e^2 + a^2 = 0. \tag{3.11}$$

The roots of the polynomial equation in Eq. (3.11) can be defined as

$$\rho_{1,2} = \frac{2ae\cos\phi\left(e^2-1\right) \pm \sqrt{\Delta}}{2\left(e^2\cos^2\phi - 1\right)} \tag{3.12}$$

where Δ is called as the discriminant of the polynomial equation. The square root of Δ can be expressed as

$$\sqrt{\Delta} = \sqrt{\left[2ae\cos\phi\left(e^2-1\right)^2\right] - 4\left(e^2\cos^2\phi - 1\right)a^2\left(e^2-1\right)^2}. \tag{3.13}$$

Finally it can be found as

$$\sqrt{\Delta} = 2a\left(e^2-1\right). \tag{3.14}$$

Then the values of ρ can be shown as

$$\rho_{1,2} = \frac{2ae\cos\phi\left(e^2-1\right)\left(e\cos\phi \pm 1\right)}{2\left(e^2\cos^2\phi - 1\right)}. \tag{3.15}$$

Due to the existence of the term $\left(e\cos\phi \pm 1\right)$ in Eq. (3.15), it can be clearly seen that there will be two different ρ values. One of them is related with the left surface of the hyperbola, the other one is related with the right surface of the hyperbola. For the term $\left(e\cos\phi + 1\right)$, ρ_1 can be defined as

$$\rho_1 = \frac{a\left(e^2-1\right)}{e\cos\phi - 1}. \tag{3.16}$$

For the second term $\left(e\cos\phi - 1\right)$, ρ_2 can be expressed as

$$\rho_2 = \frac{a\left(e^2-1\right)}{e\cos\phi + 1}. \tag{3.17}$$

It can be seen from Eq. (3.16) and Eq. (3.17) that ρ_1 and ρ_2 change when the parameters a, e and $\phi \in [0, 2\pi]$ change.

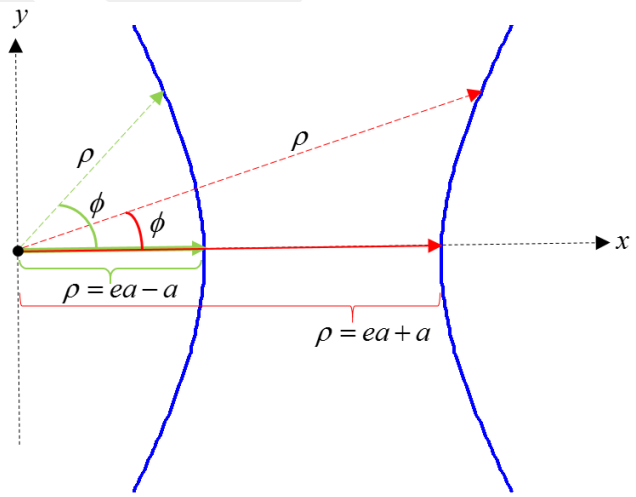

Figure 4 Values of ρ in terms of the hyperbola parameters e, a at $\phi = 0$

Figure 4 shows two ρ values in terms of the parameters e (eccentricity) and a (the distance from the center of the hyperbola to one surface) which are respectively equal to the distances of $(ea-a)$ and $(ea+a)$ when ϕ is equal to zero. These distances are individually related with either ρ_1 or ρ_2 given in Eq. (3.16) and Eq. (3.17) . The most important point is the determination of the exact ρ. The determination can be made by giving the numeric values for ϕ, a and e in ρ_1 and ρ_2. When ϕ, a and e are selected as the numeric values of $0,2$ and 3, respectively, distances of $(ea-a)$ and $(ea+a)$ can be evaluated as

$$ea-a=4 \tag{3.18}$$

and

$$ea+a=8 \tag{3.19}$$

respectively. By using the same numeric values, ρ_1 and ρ_2 in Eq. (3.16) and Eq. (3.17) are obtained as

$$\rho_1=8 \tag{3.20}$$

and

$$\rho_2=4 \tag{3.21}$$

respectively. Considering Eq. (3.18), Eq. (3.19), Eq. (3.20) and Eq. (3.21), it can be seen that ρ_1 and the distance $(ea+a)$ are equal to each other as well as ρ_2 and the distance $(ea-a)$ are equal to each other. As a result, since the distance $(ea+a)$ is related with the convex (right) surface of the hyperbola, ρ_1 can be determined as the exact ρ which can be expressed as

$$\rho=\frac{a\left(e^2-1\right)}{e\cos\phi-1}. \tag{3.22}$$

The exact ρ can also be determined by plotting ρ_1 and ρ_2 respectively in Eq. (3.16) and Eq. (3.17).

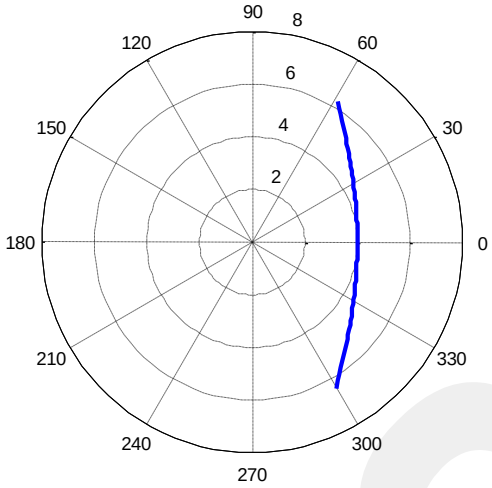

Figure 5 Polar graph of the surface equation ρ_2

Figure 5 shows the graph of ρ_2 in Eq. (3.17) where the hyperbola is placed at $\phi \in \left[-\frac{\pi}{3}, \frac{\pi}{3}\right]$. It can be seen from Fig. 5 that ρ_2 gives the concave (left) surface of the hyperbola. It can also be observed from Fig. 5 that the result in Eq. (3.21) can be verified by considering $\phi = 0$ where the graph passes from 4 that is the same result in Eq. (3.21).

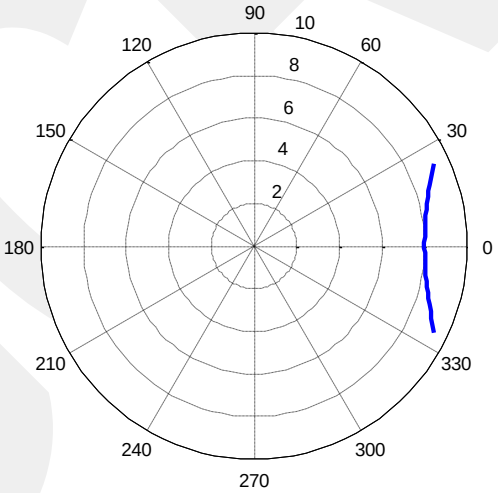

Figure 6 Polar graph of the surface equation ρ_1

Figure 6 shows the graph of ρ_1 in Eq. (3.16) where the hyperbola is placed at $\phi \in \left[-\frac{\pi}{7}, \frac{\pi}{7}\right]$. It can be seen from Fig. 6 that ρ_1 gives the convex (right) surface of the hyperbola. It can also be observed from Fig. 6 that the result in Eq. (3.20) can be

verified by considering $\phi = 0$ where the graph passes from 8 that is the same result in Eq. (3.20). As a result, by giving the numeric values and plotting the polar graphs, the exact ρ was determined as the result in Eq. (3.22).

CHAPTER 4

SCATTERING THROUGH THE HYPERBOLIC REFLECTOR

4.1 Geometry

The definition of the parameters on the geometry of a scatterer has a great importance for scattering problems. The integrals of MTPO and PO are constructed in terms of these parameters on the geometry. The evaluations of the fields of geometrical optics, nonuniform edge diffraction and uniform diffraction also depend on the scatterer geometry.

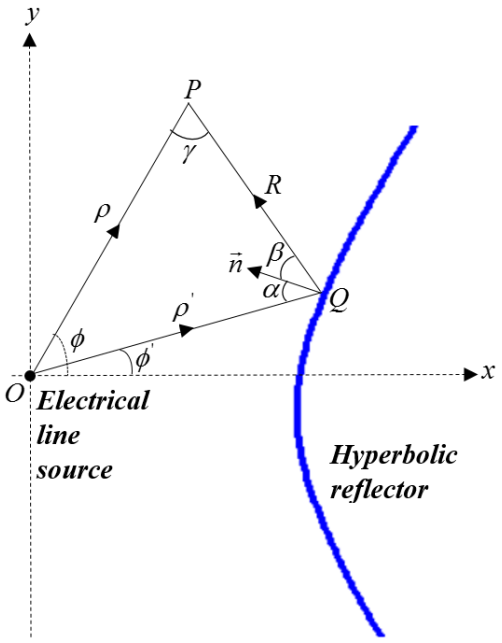

Figure 7 Basic geometry at the reflection point of the hyperbolic reflector

Figure 7 shows the basic geometry at point Q of the hyperbolic reflector. There are several parameters in Fig. 7 which are essential to define the scattering integral. From the prime parameters, ρ' is the path from the origin to the reflector surface and ϕ' is the angle between x axis and the path ρ', respectively. The prime expression comes

from the logic in antenna problems. It defines the position of the antenna element according to the origin (source). ρ and ϕ being the cylindrical coordinate parameters define the position of the observation point (P) according to the origin (source). R is named as the ray path which is the distance between the observation point (P) and the antenna element. α and β are the angles of incidence and reflection, respectively. γ is the angle between ρ and R. $\vec{n}$ is the normal vector.

4.2 Definition of the Scattering Integral

In the previous chapter, the exact ρ was evaluated. It is important both for the definition of the geometry and the definition of the unit vector of the system. Since ρ is the path from source to antenna, it should be defined in terms of the prime parameters. As a result, Eq. (3.22) will turn into its new form that can be defined as

$$\rho' = \frac{a\left(e^2 - 1\right)}{e\cos\phi' - 1}. \tag{4.1}$$

The definition of unit vector $(\vec{n})$ can be given by

$$\vec{n} = \frac{\nabla f}{\|\nabla f\|} \tag{4.2}$$

where f is zero equality of Eq. (4.1) that can be written as

$$f = a\left(e^2 - 1\right) - \rho'\left(e\cos\phi' - 1\right). \tag{4.3}$$

∇f, which is named as the gradient of f is the derivative of f according to related coordinate system. $\|\nabla f\|$ is also the magnitude of ∇f. ∇f can be generalized as

$$\nabla f = \frac{1}{h_{\rho'}}\frac{\partial f}{\partial \rho'}\vec{e}_{\rho} + \frac{1}{h_{\phi'}}\frac{\partial f}{\partial \phi'}\vec{e}_{\phi} + \frac{1}{h_{z'}}\frac{\partial f}{\partial z'}\vec{e}_{z} \tag{4.4}$$

where $h_{\rho'}$ $h_{\phi'}$ and $h_{z'}$ are the metrics of the cylindrical coordinate system. The metric of a coordinate system can be found by

$$h_i = \left\|\frac{d\vec{r}}{di}\right\| \tag{4.5}$$

where i and $\vec{r}$ are any component of a coordinate system and the sum of any coordinate system vectors, respectively. Since the metrics related with length component are always equal to 1, $h_{\rho'}$ and $h_{z'}$ are equal to 1. The metric $h_{\phi'}$, which is the metric of angle component can be found as

$$h_{\phi'} = \rho'. \tag{4.6}$$

After the evaluation of $h_{\phi'}$, ∇f can be defined as

$$\nabla f = \vec{e}_{\rho}\left(1 - e\cos\phi'\right) + \vec{e}_{\phi} e\sin\phi'. \tag{4.7}$$

$\|\nabla f\|$ can also be obtained as

$$\|\nabla f\| = \sqrt{e^2 + 1 - 2e\cos\phi'}. \tag{4.8}$$

Finally, the unit vector $\vec{n}$ can be obtained as

$$\vec{n} = \frac{1 - e\cos\phi'}{\sqrt{e^2 + 1 - 2e\cos\phi'}}\vec{e}_{\rho} + \frac{e\sin\phi'}{\sqrt{e^2 + 1 - 2e\cos\phi'}}\vec{e}_{\phi}. \tag{4.9}$$

The hyperbolic reflector is fed by an electrical line source. The electrical field of the source can be given as

$$\vec{E}_i = \vec{e}_z E_0 \frac{e^{-jk\rho}}{\sqrt{k\rho}} \tag{4.10}$$

where k being the wave number has the equation of

$$k = \frac{\omega}{c} \tag{4.11}$$

where ω and c are the angular frequency and the light velocity respectively. E_0 can be defined as

$$E_0 = e^{j\frac{\pi}{4}} \frac{\omega\mu_0 I_0}{2\sqrt{2\pi}} \tag{4.12}$$

where I_0 and μ_0 are the current of the source and permeability of the free space, respectively. The incident magnetic field can also be found by the Maxwell-Faraday equation which can be given as

$$\vec{H}_i = -\frac{1}{j\omega\mu_0}\nabla \times \vec{E}_i. \tag{4.13}$$

By using Eq. (4.13), $\vec{H}_i$ can be expressed as

$$\vec{H}_i = -\frac{1}{j\omega\mu_0\rho}\begin{vmatrix} \vec{e}_\rho & \rho\vec{e}_\phi & \vec{e}_z \\ \frac{\partial}{\partial\rho} & 0 & 0 \\ 0 & 0 & E_0\frac{e^{-jk\rho}}{\sqrt{k\rho}} \end{vmatrix} \tag{4.14}$$

where it can be seen that the result only comes from the second column of the determinant, so $\vec{H}_i$ can be defined as

$$\vec{H}_i = \vec{e}_\phi \frac{E_0}{j\omega\mu_0}\left(\frac{jke^{-jk\rho}}{\rho^{1/2}\sqrt{k}} + \frac{e^{-jk\rho}}{2\rho^{3/2}\sqrt{k}}\right) \tag{4.15}$$

where the second term having $\rho^{3/2}$ can be neglected due to its small contribution to the field. As a result, $\vec{H}_i$ can be obtained as

$$\vec{H}_i \approx \vec{e}_\phi \frac{E_0}{Z_0}\frac{e^{-jk\rho}}{\sqrt{k\rho}} \tag{4.16}$$

where Z_0 is the impedance of the free space that can be written as

$$Z_0 = \sqrt{\frac{\mu_0}{\varepsilon_0}} \tag{4.17}$$

where μ_0 and ε_0 refers to permeability and permittivity of the free space.

In this step, the magnetic vector potential $\vec{A}$ will be written since it is the transition expression for the electric and magnetic fields. The magnetic vector potential can be written as

$$\vec{A} = \frac{\mu_0}{4\pi}\iint_s \vec{J}_{MTPO}\frac{e^{-jkR_1}}{R_1}dS' \tag{4.18}$$

where R_1 and $\vec{J}_{MTPO}$ are the ray path from the surface to observation point and the surface current density that can be respectively given as

$$R_1 = \sqrt{\rho^2 + \left(\rho'\right)^2 - 2\rho\rho'\cos\left(\phi - \phi'\right) + \left(z - z'\right)^2} \tag{4.19}$$

and

$$\vec{J}_{MTPO} = \vec{n}_1 \times \vec{H}_t\big|_s \tag{4.20}$$

where $\vec{n}_1$ and $\vec{H}_t$ are the modified unit vector and the total magnetic field, respectively. The term $\frac{e^{-jkR_1}}{R_1}$ is named as Green function. $dS^{'}$ can be given by

$$dS^{'} = \frac{\rho^{'}}{\vec{n}\vec{e}_{\rho}} d\phi^{'} dz^{'}, \tag{4.21}$$

which can also be defined as

$$dS^{'} = \frac{\rho^{'}\sqrt{e^2 + 1 - 2e\cos\phi^{'}}}{1 - e\cos\phi^{'}} d\phi^{'} dz^{'}. \tag{4.22}$$

The magnetic vector potential has a relation with the electric and magnetic fields. The relation between the electric field and the magnetic vector potential can be shown as

$$\vec{E} \approx -j\omega\vec{A}. \tag{4.23}$$

The connection between the magnetic field and the magnetic vector potential can also be shown as

$$\vec{H} = \frac{1}{\mu_0}\nabla \times \vec{A}. \tag{4.24}$$

Then the magnetic vector potential as in Ref. [37] can be given by

$$\vec{A} = \vec{e}_z \frac{\mu_0}{4\pi} \int_{\phi^{'}=-\phi_0}^{\phi_0} \int_{z^{'}=-\infty}^{\infty} f(\alpha,\beta) \frac{E_0}{Z_0} \frac{e^{-jk\rho^{'}}}{\sqrt{k\rho}} \frac{e^{-jkR_1}}{R_1} \frac{\rho^{'}}{\vec{n}\vec{e}_{\rho}} d\phi^{'} dz^{'} \tag{4.25}$$

where the term $f(\alpha,\beta)$, which comes from the new unit vector expression as in Ref. [37] can be expressed as

$$f(\alpha,\beta) = \sin\left(\frac{\beta+\alpha}{2}\right) - \sin\left(\frac{\beta-\alpha}{2}\right). \tag{4.26}$$

For this study, since the parameters α and β are used as the complement of $\frac{\pi}{2}$, this expression can be redefined as

$$f(\alpha,\beta) = \cos\left(\frac{\beta+\alpha}{2}\right) - \sin\left(\frac{\alpha-\beta}{2}\right). \tag{4.27}$$

The part $z^{'}$ of the integral can be eliminated as in Ref. [32]. The term R_1 can be defined as

$$R_1 = \sqrt{R^2 + \left(z - z^{'}\right)^2}. \tag{4.28}$$

The z' part of the integral in Eq. (4.25) can be eliminated by using the variable change of $\left(z-z'\right)=R\sinh\alpha$ where R is equal to $\sqrt{\rho^2+\left(\rho'\right)^2-2\rho\rho'\cos\left(\phi-\phi'\right)}$. The z' part in Eq. (4.25) can be simplified as

$$\int_c e^{-jk\cosh\alpha}d\alpha=\frac{\pi}{j}H_0^{(2)}\left(kR\right) \tag{4.29}$$

where the Hankel function can be expressed as

$$H_0^{(2)}\left(kR\right)\approx\sqrt{\frac{2}{\pi}}e^{j\frac{\pi}{4}}\frac{e^{-jkR}}{\sqrt{kR}}. \tag{4.30}$$

Then the scattering integral of MTPO as in Ref. [37] can be written as

$$\vec{E}_s=\vec{e}_z E_0\frac{e^{-jk\rho}}{\sqrt{k\rho}}+\vec{e}_z E_0\frac{ke^{j\frac{\pi}{4}}}{\sqrt{2\pi}}\int_{\phi'=-\phi_0}^{\phi_0} f\left(\alpha,\beta\right)\frac{e^{-jk\rho'}}{\sqrt{k\rho'}}\frac{e^{-jkR}}{\sqrt{kR}}\frac{\rho'}{\vec{n}\vec{e}_\rho}d\phi' \tag{4.31}$$

4.3 Asymptotic Evaluation of the Scattering Integral

In this section, the scattering integral in Eq. (4.31) will be asymptotically evaluated using the method of stationary phase and the edge point technique. Firstly, the method of the stationary phase will be introduced. It can be applied to the general integral form that can be given by

$$I=\int_a^b f\left(\phi'\right)e^{-jkg\left(\phi'\right)}d\phi' \tag{4.32}$$

where ϕ', $f\left(\phi'\right)$ and $g\left(\phi'\right)$ are the variables of the integral being the amplitude function of the integral and the phase function of the integral, respectively. There are also a and b which are the upper and lower limits of the integral. The application of the method begins with the definition of the phase function because the method depends on the expansion of the first three terms of Taylor series. There will be the stationary phase point which is named as ϕ_s. It can be found by the evaluation of the first derivative of the phase function. The general form of the phase function can be given as

$$g\left(\phi'\right)=\rho'+R \tag{4.33}$$

where R is the ray path that can be defined as

$$R = \rho \cos\gamma + \rho' \cos(\alpha + \beta). \tag{4.34}$$

The phase function can be redefined as

$$g(\phi') = \rho' + \rho \cos\gamma + \rho' \cos(\alpha + \beta), \tag{4.35}$$

which can be rearranged as

$$g(\phi') = \rho \cos\gamma + \rho' \left[1 + \cos(\alpha + \beta)\right]. \tag{4.36}$$

In this step, the first derivative of the phase function will be evaluated. It can be written as

$$\frac{dg}{d\phi'} = \frac{d\rho'}{d\phi'} + \frac{dR}{d\phi'}, \tag{4.37}$$

which can be redefined as

$$\frac{dg}{d\phi'} = \frac{d\rho'}{d\phi'} + \frac{d}{d\phi'}\left[\rho \cos\gamma + \rho' \cos(\alpha + \beta)\right]. \tag{4.38}$$

The first derivative of R can be expressed as

$$\frac{dR}{d\phi'} = -\rho \sin\gamma \frac{d\gamma}{d\phi'} + \cos(\alpha + \beta)\frac{d\rho'}{d\phi'} + \rho' \frac{d}{d\phi'}\left(\cos(\alpha + \beta)\right) \tag{4.39}$$

where γ can be expressed as

$$\gamma = \pi + \phi - \phi' - \alpha - \beta. \tag{4.40}$$

The first derivative of γ can be defined as

$$\frac{d\gamma}{d\phi'} = 1 - \frac{d\alpha}{d\phi'} - \frac{d\beta}{d\phi'}. \tag{4.41}$$

After that, the first derivative of the phase function can be redefined as

$$\frac{dg}{d\phi'} = \frac{d\rho'}{d\phi'} - \rho \sin\gamma \frac{d\gamma}{d\phi'} + \frac{d\rho'}{d\phi'}\cos(\alpha + \beta) - \rho' \sin(\alpha + \beta)\left(\frac{d\beta}{d\phi'} + \frac{d\alpha}{d\phi'}\right). \tag{4.42}$$

In order to simplify Eq. (4.42), the sine rule can be written as

$$\frac{\rho'}{\sin\gamma} = \frac{\rho}{\sin(\alpha + \beta)}. \tag{4.43}$$

By using Eq. (4.43), the first derivative of the phase function can be obtained as

$$\frac{dg}{d\phi'} = \frac{d\rho'}{d\phi'}\left(1 + \cos(\alpha + \beta)\right) - \rho \sin(\alpha + \beta) \tag{4.44}$$

where $\frac{d\rho'}{d\phi'}$ can be defined as

$$\frac{d\rho^{'}}{d\phi^{'}} = \rho^{'}\frac{e\sin\phi^{'}}{e\cos\phi^{'}-1}, \tag{4.45}$$

which can be written in Eq. (4.44). Then the first derivative of the phase function can be expressed as

$$\frac{dg}{d\phi^{'}} = \frac{\rho^{'}}{e\cos\phi^{'}-1}\left[e\sin\phi^{'} + e\sin\left(\phi^{'}-\alpha-\beta\right)+\sin\left(\alpha+\beta\right)\right]. \tag{4.46}$$

The stationary phase points which are named as ϕ_s points that makes the first derivative of the phase function equal to zero. In order to find them, some applications will be applied to the first derivative of the phase function. First of all, the relation among $\phi^{'}$, α and β should be expressed. By using the geometry given in Fig. 7, the relation between $\phi^{'}$ and α can be given by

$$\vec{n}.\vec{e}_{\rho} = \cos\left(\pi-\alpha\right), \tag{4.47}$$

which can be expressed as

$$\left(\frac{1-e\cos\phi^{'}}{\sqrt{e^2+1-2e\cos\phi^{'}}}\vec{e}_{\rho} + \frac{e\sin\phi^{'}}{\sqrt{e^2+1-2e\cos\phi^{'}}}\vec{e}_{\phi}\right).\vec{e}_{\rho} = \frac{1-e\cos\phi^{'}}{\sqrt{e^2+1-2e\cos\phi^{'}}}. \tag{4.48}$$

As a result, the relation between $\phi^{'}$ and α can be obtained as

$$\cos\alpha = \frac{e\cos\phi^{'}-1}{\sqrt{e^2+1-2e\cos\phi^{'}}}. \tag{4.49}$$

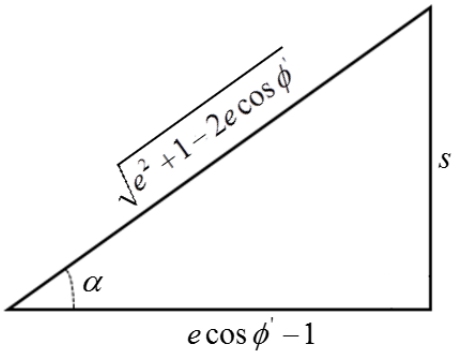

Figure 8 Representation of the cosine of α on the right angled triangle

Figure 8 shows the cosine of α on the right angled triangle by which the sine or tangent of α can be obtained. The Pythagorean relation for the other side s can be written as

$$\left(e\cos\phi^{'}-1\right)^{2}+s^{2}=\left(\sqrt{e^{2}+1-2e\cos\phi^{'}}\right)^{2} \tag{4.50}$$

where s can be found as

$$s=e\sin\phi^{'}. \tag{4.51}$$

After this evaluation, the sine of α can be written as

$$\sin\alpha=\frac{e\sin\phi^{'}}{\sqrt{e^{2}+1-2e\cos\phi^{'}}}. \tag{4.52}$$

The tangent of α can also be written as

$$\tan\alpha=\frac{e\sin\phi^{'}}{e\cos\phi^{'}-1}. \tag{4.53}$$

Eq. (4.53) can be used in the first derivative of the phase function in order to find the stationary phase points. The first derivative of the phase function can be arranged as

$$\frac{dg}{d\phi^{'}}=\rho^{'}\left\{\frac{e\sin\phi^{'}}{e\cos\phi^{'}-1}\left[1+\cos\left(\alpha+\beta\right)\right]-\sin\left(\alpha+\beta\right)\right\}, \tag{4.54}$$

which includes the term of the tangent of α found in Eq. (4.53) by which Eq. (4.54) can be rearranged as

$$\frac{dg}{d\phi^{'}}=\rho^{'}\left\{\tan\alpha\left[1+\cos\left(\alpha+\beta\right)\right]-\sin\left(\alpha+\beta\right)\right\}. \tag{4.55}$$

Just as the stationary phase point of $\phi^{'}$ is named as ϕ_{s}, the stationary phase points of α and β are named as α_{s} and β_{s}, respectively. In this step, the stationary phase values of β_{s} will be found. Eq. (4.55) can be written as

$$\frac{dg}{d\phi^{'}}=\rho^{'}\left\{\frac{\sin\alpha}{\cos\alpha}\left[1+\cos\left(\alpha+\beta\right)\right]-\sin\left(\alpha+\beta\right)\right\}, \tag{4.56}$$

which can also be redefined as

$$\frac{dg}{d\phi^{'}}=\frac{2\rho^{'}}{\cos\alpha}\cos\left(\frac{\beta+\alpha}{2}\right)\left[\sin\alpha\cos\left(\frac{\beta+\alpha}{2}\right)-\cos\alpha\sin\left(\frac{\beta+\alpha}{2}\right)\right]. \tag{4.57}$$

Finally, the first derivative of the phase function can be arranged as

$$\frac{dg}{d\phi^{'}}=\frac{2\rho^{'}}{\cos\alpha}\cos\left(\frac{\beta+\alpha}{2}\right)\sin\left(\frac{\alpha-\beta}{2}\right). \tag{4.58}$$

In this stage, the stationary phase points of the scattering integral can be found by equating the first derivative of the phase function to zero. Equating to zero is satisfied

when the terms of $\sin\left(\frac{\alpha-\beta}{2}\right)$ and $\cos\left(\frac{\beta+\alpha}{2}\right)$ are separately equal to zero. Initially, the sine term will be investigated. It can be written as

$$\sin\left(\frac{\alpha-\beta}{2}\right)=0. \tag{4.59}$$

In order to satisfy equating to zero, the sine term inside should be equal to zero due to the basic sine function property. It can be given by

$$\frac{\alpha-\beta}{2}=0. \tag{4.60}$$

As a result, the first stationary phase value of β can be found as

$$\beta_s=\alpha_s \tag{4.61}$$

Then the second stationary phase value of β can be found by using the cosine term. It can be written as

$$\cos\left(\frac{\beta+\alpha}{2}\right)=0. \tag{4.62}$$

In order to satisfy equating to zero, the cosine term inside should be equal to $(2n+1)\frac{\pi}{2}, n\in\mathbb{Z}$ due to the basic cosine function property. It can be given by

$$\frac{\beta+\alpha}{2}=(2n+1)\frac{\pi}{2}. \tag{4.63}$$

For $n=0$, it can be given by

$$\frac{\beta+\alpha}{2}=\frac{\pi}{2}. \tag{4.64}$$

Finally, the second stationary phase value of β can be found as

$$\beta_s=\pi-\alpha_s \tag{4.65}$$

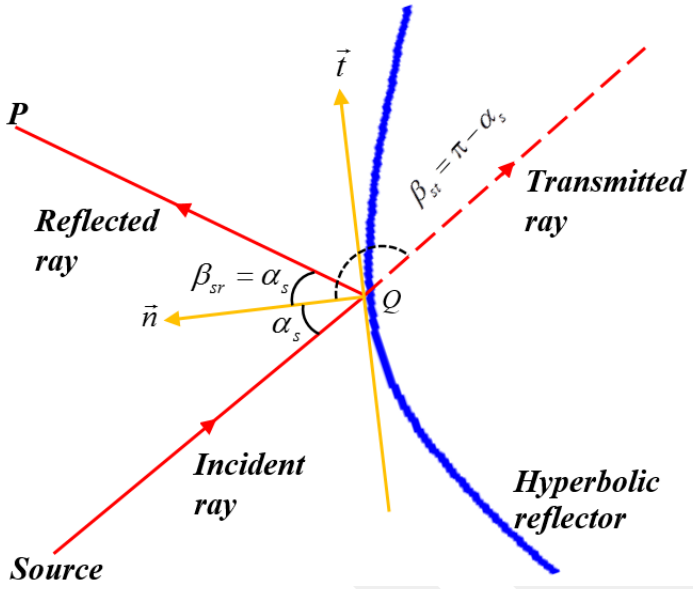

Figure 9 Stationary phase geometry of the reflected and transmitted rays

Figure 9 shows the stationary phase geometry of the reflected and transmitted rays. It can be seen from the Fig. 9 that the values of β_s in Eq. (4.61) and Eq. (4.65) are related with the reflected and transmitted scattered waves, respectively.

After the evaluations of the stationary phase points, the next step is the evaluation of the second derivative of the phase function since the method of stationary phase uses the first three terms of Taylor series which include the second derivative. The general Taylor series representation can be expressed as

$$\sum_{n=0}^{\infty} \frac{g^{(n)}(\phi_s)}{n!}\left(\phi' - \phi_s\right)^n \tag{4.66}$$

where the first three terms can be defined as

$$\sum_{n=0}^{2} \frac{g^{(n)}(\phi_s)}{n!}\left(\phi' - \phi_s\right)^n = \frac{g(\phi_s)}{0!} + \frac{g^{(1)}(\phi_s)}{1!}\left(\phi' - \phi\right) + \frac{g^{(2)}(\phi_s)}{2!}\left(\phi' - \phi_s\right)^2. \tag{4.67}$$

Thus, the phase function can be approximated as

$$g\left(\phi'\right) \sim g(\phi_s) + g^{(1)}(\phi_s)\left(\phi' - \phi\right) + \frac{g^{(2)}(\phi_s)}{2}\left(\phi' - \phi_s\right)^2 \tag{4.68}$$

where the first derivative gives the result of zero since ϕ_s points are found by equating the first derivative of the phase function to zero. Thus, the term of the first derivative in Eq. (4.68) will normally be eliminated. As a result, the phase function can be simplified as

$$g\left(\phi'\right) \approx g\left(\phi_s\right) + \frac{g^{(2)}\left(\phi_s\right)}{2}\left(\phi' - \phi_s\right)^2. \tag{4.69}$$

In this stage, the second derivative of the phase function will be found. It can be obtained by taking the derivative of the first derivative of the phase function. The second derivative can be given by

$$\frac{d^2 g}{d\left(\phi'\right)^2} = \frac{d}{d\phi'}\left(\frac{dg}{d\phi'}\right). \tag{4.70}$$

In order to easily evaluate the second derivative, the first derivative of the phase function in Eq. (4.58) can be rearranged as

$$\frac{dg}{d\phi'} = \rho'\left(\frac{\sin\alpha - \sin\beta}{\cos\alpha}\right). \tag{4.71}$$

The second derivative of the phase function can be defined as

$$\frac{d^2 g}{d\left(\phi'\right)^2} = \frac{d\rho'}{d\phi'}\left(\frac{\sin\alpha - \sin\beta}{\cos\alpha}\right)$$

$$+\rho'\left[\frac{\left(\cos\alpha\frac{d\alpha}{d\phi'} - \cos\beta\frac{d\beta}{d\phi'}\right)\cos\alpha + \left(\sin\alpha - \sin\beta\right)\sin\alpha\frac{d\alpha}{d\phi'}}{\cos^2\alpha}\right]. \tag{4.72}$$

In this step, the part of general scattering integral of MTPO which is named as $\vec{E}$ represents the parts of reflected and transmitted fields. It can be written as

$$\vec{E} = -\vec{e}_z E_0 \frac{k e^{j\frac{\pi}{4}}}{\sqrt{2\pi}}\left[\int_{\phi'=-\phi_0}^{\phi_0} \cos\left(\frac{\beta+\alpha}{2}\right)\frac{e^{-jk\rho'}}{\sqrt{k\rho'}}\frac{e^{-jkR}}{\sqrt{kR}}\frac{\rho'}{\cos\alpha}d\phi'\right.$$

$$\left. + \int_{\phi'=-\phi_0}^{\phi_0} \sin\left(\frac{\alpha-\beta}{2}\right)\frac{e^{-jk\rho'}}{\sqrt{k\rho'}}\frac{e^{-jkR}}{\sqrt{kR}}\frac{\rho'}{\cos\alpha}d\phi'\right], \tag{4.73}$$

which can also be defined as

$$\vec{E} = -\vec{e}_z E_0 \frac{k e^{j\frac{\pi}{4}}}{\sqrt{2\pi}}\left(M_1 + M_2\right) \tag{4.74}$$

where M_1 and M_2 are related with the integrals of the fields of reflected and transmitted, respectively. M_1 can be defined as

$$M_1 = \int_{\phi'=-\phi_0}^{\phi_0} \cos\left(\frac{\beta+\alpha}{2}\right)\frac{e^{-jk\rho'}}{\sqrt{k\rho'}}\frac{e^{-jkR}}{\sqrt{kR}}\frac{\rho'}{\cos\alpha}d\phi', \tag{4.75}$$

which is related with the reflected field. The first β_s value in Eq. (4.61) will be used in this integral. M_2 can also be defined as

$$M_2 = \int_{\phi'=-\phi_0}^{\phi_0} \sin\left(\frac{\alpha-\beta}{2}\right)\frac{e^{-jk\rho'}}{\sqrt{k\rho'}}\frac{e^{-jkR}}{\sqrt{kR}}\frac{\rho'}{\cos\alpha}d\phi', \tag{4.76}$$

which is related with the transmitted field. The second β_s value in Eq. (4.65) will be used in this integral. The integrals of M_1 and M_2 will be asymptotically evaluated. The general representation of the stationary phase equivalents of the amplitude and phase function can be expressed as

$$f\left(\phi'\right) \approx f\left(\phi_s\right) \tag{4.77}$$

and

$$g\left(\phi'\right) \approx g\left(\phi_s\right) + \frac{1}{2}\frac{d^2 g\left(\phi_s\right)}{d\left(\phi'\right)^2}\left(\phi'-\phi_s\right)^2 \tag{4.78}$$

respectively. ϕ_s is related with the values of β_s which are equal to α_s and $\pi-\alpha_s$ for the reflected and transmitted fields, respectively.

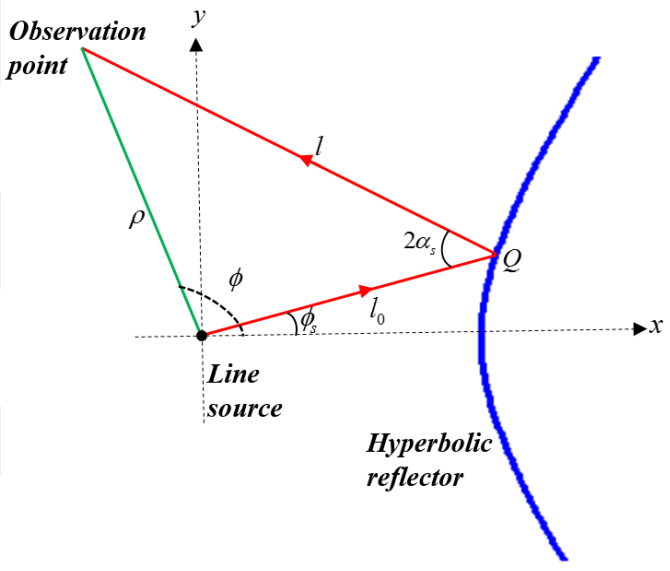

Figure 10 Reflection geometry at the stationary phase point

Figure 10 shows the reflection geometry at point Q. There are the reflection parameters of l_0 and l which are related with $\rho'(\phi_s')$ and $R(\phi_s')$, respectively. Firstly, the reflected GO field will be evaluated from M_1. The amplitude and phase functions of M_1 can be written as

$$f(\phi') = \frac{\cos\left(\frac{\beta+\alpha}{2}\right)}{\cos\alpha}\frac{1}{\sqrt{k\rho'}}\frac{1}{\sqrt{kR}}\rho' \tag{4.79}$$

and

$$g(\phi') = \rho' + R \tag{4.80}$$

respectively. For the reflection stationary phase point β_s value which is equal to α_s, the amplitude function can be expressed as

$$f(\phi_s') \approx \frac{\rho'(\phi_s')}{\sqrt{k\rho'(\phi_s')}\sqrt{kR(\phi_s')}}. \tag{4.81}$$

By using the reflection parameters, the amplitude function can be written as

$$f(\phi_s') \approx \frac{l_0}{\sqrt{kl_0}\sqrt{kl}}. \tag{4.82}$$

When β_s is inserted, the second derivative term of the phase function in Taylor expansion can be reduced as

$$\frac{d^2g}{d(\phi')^2} = \frac{l_0}{\cos\alpha_s}\frac{d\alpha}{d\phi'} - l_0\frac{d\beta}{d\phi'} \tag{4.83}$$

where the first derivative of β should be evaluated. The derivative of Eq. (4.43) can be written as

$$\frac{d\rho'}{d\phi'}\sin(\alpha+\beta) + \rho'\cos(\alpha+\beta)\left[\frac{d\alpha}{d\phi'} + \frac{d\beta}{d\phi'}\right] = \rho\cos\gamma\frac{d\gamma}{d\phi'} \tag{4.84}$$

where $\frac{d\gamma}{d\phi'}$ was found in Eq. (4.41) by which Eq. (4.85) can be redefined as

$$\frac{d\rho'}{d\phi'}\sin(\alpha+\beta) + \rho'\cos(\alpha+\beta)\left[\frac{d\alpha}{d\phi'} + \frac{d\beta}{d\phi'}\right] = \rho\cos\gamma\left[1 - \left[\frac{d\alpha}{d\phi'} + \frac{d\beta}{d\phi'}\right]\right], \tag{4.85}$$

which can be rearranged as

$$\frac{d\rho^{'}}{d\phi^{'}}\sin(\alpha+\beta)+\left[\rho^{'}\cos(\alpha+\beta)+\rho\cos\gamma\right]\left[\frac{d\alpha}{d\phi^{'}}+\frac{d\beta}{d\phi^{'}}\right]=\rho\cos\gamma \qquad (4.86)$$

where $\left[\rho^{'}\cos(\alpha+\beta)+\rho\cos\gamma\right]$ is equal to R which was found in Eq. (4.34) and $\frac{d\rho^{'}}{d\phi^{'}}$ can be written as

$$\frac{d\rho^{'}}{d\phi^{'}}=\rho^{'}\tan\alpha. \qquad (4.87)$$

By using Eq. (4.34) and Eq. (4.87), Eq. (4.86) can be redefined as

$$R\left[\frac{d\alpha}{d\phi^{'}}+\frac{d\beta}{d\phi^{'}}\right]=\rho\cos\gamma-\rho^{'}\tan\alpha\sin(\alpha+\beta), \qquad (4.88)$$

which can be written as

$$R\left[\frac{d\alpha}{d\phi^{'}}+\frac{d\beta}{d\phi^{'}}\right]=R-\rho^{'}\left[\frac{\cos(\alpha+\beta)\cos\alpha+\sin(\alpha+\beta)\sin\alpha}{\cos\alpha}\right], \qquad (4.89)$$

which can also be redefined as

$$R\left[\frac{d\alpha}{d\phi^{'}}+\frac{d\beta}{d\phi^{'}}\right]=R-\rho^{'}\frac{\cos\beta}{\cos\alpha}, \qquad (4.90)$$

which can be arranged as

$$\frac{d\alpha}{d\phi^{'}}+\frac{d\beta}{d\phi^{'}}=1-\frac{\rho^{'}}{R}\frac{\cos\beta}{\cos\alpha}. \qquad (4.91)$$

Finally, the first derivative of β can be defined as

$$\frac{d\beta}{d\phi^{'}}=1-\frac{\rho^{'}}{R}\frac{\cos\beta}{\cos\alpha}-\frac{d\alpha}{d\phi^{'}}. \qquad (4.92)$$

After this evaluation, the second derivative of the phase function for the reflection can be rewritten as

$$\frac{d^2g}{d\left(\phi^{'}\right)^2}=l_0\left(2\frac{d\alpha}{d\phi^{'}}+\frac{l_0}{l}-1\right). \qquad (4.93)$$

The phase function for the reflection can be written as

$$g\left(\phi^{'}\right)\approx l+l_0+\frac{1}{2}l_0\left(2\frac{d\alpha}{d\phi^{'}}+\frac{l_0}{l}-1\right)\left(\phi^{'}-\phi_s\right)^2 \qquad (4.94)$$

where the first derivative of α can be found by using Eq. (4.58). It can be evaluated as

$$\frac{d\alpha}{d\phi'} = \frac{e^2 - e\cos\phi_s}{e^2 + 1 - 2e\cos\phi_s}. \tag{4.95}$$

In this stage, in order to complete the asymptotic evaluation of the integral, the error function can be used. The error function can be expressed as

$$\int_{-\infty}^{\infty} e^{-\frac{y^2}{2}} dy = \sqrt{2\pi} \tag{4.96}$$

where the power of the exponential function and the phase function in Eq. (4.96) will be equated to each other. The aim is to find $d\phi'$ which can be found by the equation of

$$-jk\frac{1}{2}l_0\left(2\frac{d\alpha}{d\phi'} + \frac{l_0}{l} - 1\right)\left(\phi' - \phi_s\right)^2 = -\frac{y^2}{2}, \tag{4.97}$$

which can be redefined as

$$\sqrt{-jk\frac{1}{2}l_0\left(2\frac{d\alpha}{d\phi'} + \frac{l_0}{l} - 1\right)\left(\phi' - \phi_s\right)^2} = \sqrt{-\frac{y^2}{2}} \tag{4.98}$$

where the term $\left(\phi' - \phi_s\right)$ can be expressed as

$$\left(\phi' - \phi_s\right) = y\frac{1}{\sqrt{j}}\frac{1}{\sqrt{k}}\frac{\sqrt{l}}{\sqrt{l_0}\sqrt{2\frac{d\alpha}{d\phi'} + l_0 - l}} \tag{4.99}$$

where the term $\frac{1}{\sqrt{j}}$ can be defined as

$$\frac{1}{\sqrt{j}} = e^{-j\frac{\pi}{4}}. \tag{4.100}$$

Finally, $d\phi'$ can be evaluated as

$$d\phi' = e^{-j\frac{\pi}{4}}\frac{1}{\sqrt{k}}\frac{\sqrt{l}}{\sqrt{l_0}}\frac{1}{\sqrt{2\frac{d\alpha}{d\phi'}l + l_0 - l}}dy. \tag{4.101}$$

After the evaluation of $d\phi'$, the result of M_1 can be rearranged as

$$M_1 \approx f\left(\phi_s\right)e^{-j\frac{\pi}{4}}\frac{1}{\sqrt{k}}\frac{\sqrt{l}}{\sqrt{l_0}}\frac{e^{-jk(l+l_0)}}{\sqrt{2\frac{d\alpha}{d\phi'}l + l_0 - l}}\int_{-\infty}^{\infty} e^{-\frac{y^2}{2}}dy \tag{4.102}$$

where the error function is equal to $\sqrt{2\pi}$. As a result, M_1 can be found as

$$M_1 \approx \frac{1}{k}\frac{\sqrt{l_0}}{\sqrt{l}}e^{-j\frac{\pi}{4}}\frac{1}{\sqrt{k}}\frac{\sqrt{l}}{\sqrt{l_0}}\frac{e^{-jk(l+l_0)}}{\sqrt{2\frac{d\alpha}{d\phi'}l+l_0-l}}\sqrt{2\pi}. \tag{4.103}$$

After the evaluation of M_1 , the next step is to find the transmitted GO field from M_2. Similar steps in the evaluation of M_1 can be applied to M_2. The difference is the stationary phase point β_s which is equal to $\pi-\alpha_s$ for the transmission. The amplitude function can be written as

$$f(\phi_s) \approx \frac{1}{\sqrt{k\rho'(\phi_s)}\sqrt{kR(\phi_s)}}\rho'(\phi_s) \tag{4.104}$$

where $\rho'(\phi_s)$ and $R(\phi_s)$ can be represented in terms of transmission parameters of ρ_s and R_s, respectively. Thus, the amplitude function can be rewritten as

$$f(\phi') \approx \frac{1}{\sqrt{k\rho_s}\sqrt{kR_s}}\rho_s. \tag{4.105}$$

When β_s is inserted, the second derivative term of the phase function in Taylor expansion can be reduced as

$$\frac{d^2g}{d\left(\phi'\right)^2} = \rho_s\left(\frac{d\alpha}{d\phi'}+\frac{d\beta}{d\phi'}\right) \tag{4.106}$$

where $\frac{d\beta}{d\phi'}$ found in Eq. (4.92) can also be used in Eq. (4.106). Then, the second derivative of the phase function can be rewritten as

$$\frac{d^2g}{d\left(\phi'\right)^2} = \rho_s\left(\frac{R_s+\rho_s}{R_s}\right). \tag{4.107}$$

The phase function for the transmission can be written as

$$g\left(\phi'\right) \approx \rho_s + R_s + \frac{1}{2}\frac{\rho_s}{R_s}\left(R_s+\rho_s\right)\left(\phi'-\phi_s\right)^2. \tag{4.108}$$

In order to complete the asymptotic evaluation of the integral, the error function can also be used as in M_1. The power of exponential function in Eq. (4.96) and the phase

function in Eq. (4.108) will be equated to each other. The aim is to find $d\phi'$ which can be found by the equation of

$$-jk\frac{1}{2}\frac{\rho_s}{R_s}\left(R_s+\rho_s\right)\left(\phi'-\phi_s\right)^2=-\frac{y^2}{2}, \tag{4.109}$$

which can be redefined as

$$\sqrt{-jk\frac{1}{2}\frac{\rho_s}{R_s}\left(R_s+\rho_s\right)\left(\phi'-\phi_s\right)^2}=\sqrt{-\frac{y^2}{2}} \tag{4.110}$$

where the term $\left(\phi'-\phi_s\right)$ can be expressed as

$$\left(\phi'-\phi_s\right)=\frac{1}{\sqrt{j}}\frac{\sqrt{R_s}}{\sqrt{\rho_s}}\frac{1}{\sqrt{R_s+\rho_s}}\frac{1}{\sqrt{k}}y. \tag{4.111}$$

Finally, $d\phi'$ can be evaluated as

$$d\phi'=e^{-j\frac{\pi}{4}}\frac{\sqrt{R_s}}{\sqrt{\rho_s}}\frac{1}{\sqrt{R_s+\rho_s}}\frac{1}{\sqrt{k}}dy. \tag{4.112}$$

After the evaluation of $d\phi'$, the result of M_2 can be rearranged as

$$M_2\approx f\left(\phi_s\right)e^{-j\frac{\pi}{4}}\frac{\sqrt{R_s}}{\sqrt{\rho_s}}\frac{1}{\sqrt{R_s+\rho_s}}\frac{1}{\sqrt{k}}\int_{-\infty}^{\infty}e^{-\frac{y^2}{2}}dy \tag{4.113}$$

where the error function is equal to $\sqrt{2\pi}$. As a result, M_2 can be found as

$$M_2\approx\frac{1}{k}e^{-j\frac{\pi}{4}}\frac{e^{-jk\left(R_s+\rho_s\right)}}{\sqrt{k\left(R_s+\rho_s\right)}}\sqrt{2\pi}. \tag{4.114}$$

After the asymptotic evaluations of M_1 and M_2, the total GO result of $\vec{E}$ can be evaluated as

$$\vec{E}=-\vec{e}_zE_0\frac{1}{\sqrt{k}}\frac{e^{-jk(l+l_0)}}{\sqrt{2\frac{d\alpha}{d\phi'}l+l_0-l}}-\vec{e}_zE_0\frac{e^{-jk\left(R_s+\rho_s\right)}}{\sqrt{k\left(R_s+\rho_s\right)}}. \tag{4.115}$$

The total asymptotic result of the scattering integral of MTPO can be written as

$$\vec{E}_s=\vec{e}_zE_0\left[\frac{e^{-jk\rho}}{\sqrt{k\rho}}-\frac{1}{\sqrt{k}}\frac{e^{-jk(l+l_0)}}{\sqrt{2\frac{d\alpha}{d\phi'}l+l_0-l}}-\frac{e^{-jk\left(R_s+\rho_s\right)}}{\sqrt{k\left(R_s+\rho_s\right)}}\right], \tag{4.116}$$

which includes the incident field given in Eq. (4.10), the reflected GO field and transmitted GO field. The result of the method of stationary phase for the reflected GO field can be written as

$$\vec{E}_r^{GO} = -\vec{e}_z E_0 \frac{1}{\sqrt{k}} \frac{e^{-jk(l+l_0)}}{\sqrt{2\frac{d\alpha}{d\phi'}l + l_0 - l}}, \tag{4.117}$$

which can also be expressed by the divergence coefficient as

$$\vec{E}_r^{GO} = -\vec{e}_z E_0 \frac{\sqrt{ll_0}}{\sqrt{k\left(2\frac{d\alpha}{d\phi'}l + l_0 - l\right)}} \frac{e^{-jk(l+l_0)}}{\sqrt{kl}\sqrt{kl_0}} \tag{4.118}$$

where the divergence coefficent that affects the amplitude level of the reflected fields can be defined as

$$D_{coeff} = \frac{\sqrt{ll_0}}{\sqrt{k\left(2\frac{d\alpha}{d\phi'}l + l_0 - l\right)}}. \tag{4.119}$$

The result of the method of stationary phase for the transmitted GO field can also be written as

$$\vec{E}_t^{GO} = -\vec{e}_z E_0 \frac{e^{-jk(\rho_s + R_s)}}{\sqrt{k(\rho_s + R_s)}}. \tag{4.120}$$

Since the hyperbolic reflector is placed at $\phi \in [-\phi_0, \phi_0]$, the transmitted fields occur in the outer of the reflector at $\phi \in [(\phi > \phi_0), (\phi < 2\pi - \phi_0)]$. Thus, the transmitted GO field can be redefined as

$$\vec{E}_t^{GO} = \vec{e}_z E_0 \frac{e^{-jk(\rho_s + R_s)}}{\sqrt{k(\rho_s + R_s)}} \left[U(\phi - \phi_0) - U(\phi - 2\pi + \phi_0)\right] \tag{4.121}$$

where U is the unit step function. It can also be seen that $\rho_s + R_s$ is equal to ρ for the outer of the reflector. This also agrees with the incident field.

4.4 Edge Diffracted Waves

In this part, the nonuniform and uniform edge diffracted fields will be evaluated. The nonuniform edge diffracted fields will be evaluated for the transmitted and reflected scattered waves by using the edge point technique. The uniform diffracted fields will be evaluated by using the method of the uniform theory of diffraction (UTD), introduced in [29], [38].

4.4.1 Nonuniform Diffracted Fields

The edge point technique can be applied to a general diffraction integral D that can be defined as

$$D = \int_m^n f(y) e^{-jKg(y)} dy \tag{4.122}$$

where $f(y)$ and $g(y)$ are the amplitude and phase functions of the diffraction integral, respectively. K is the large parameter. Since the multiplying and dividing by a same term cannot affect the equation, Eq. (4.122) can be redefined as

$$D = \int_m^n \frac{f(y)}{g'(y)} g'(y) e^{-jKg(y)} dy \tag{4.123}$$

where the amplitude function was multiplied and divided by the first derivative of the phase function. In Eq. (4.123), the rule of the integration by parts can be applied as

$$D = \frac{1}{jK}\left[\frac{f(m)}{g'(m)} e^{-jKg(m)} - \frac{f(n)}{g'(n)} e^{-jKg(n)}\right] + \frac{1}{jK}\int_m^n \frac{f(y)g(x) - f(y)g'(x)}{\left[g'(y)\right]^2} e^{-jKg(y)} dy \tag{4.124}$$

where the rigth part of the Eq. (4.125) can be neglected for the large values of K. Consequently, the general equation of the edge point technique can be obtained as

$$D = \frac{1}{jK}\frac{f(m)}{g'(m)} e^{-jKg(m)} - \frac{1}{jK}\frac{f(n)}{g'(n)} e^{-jKg(n)} \tag{4.125}$$

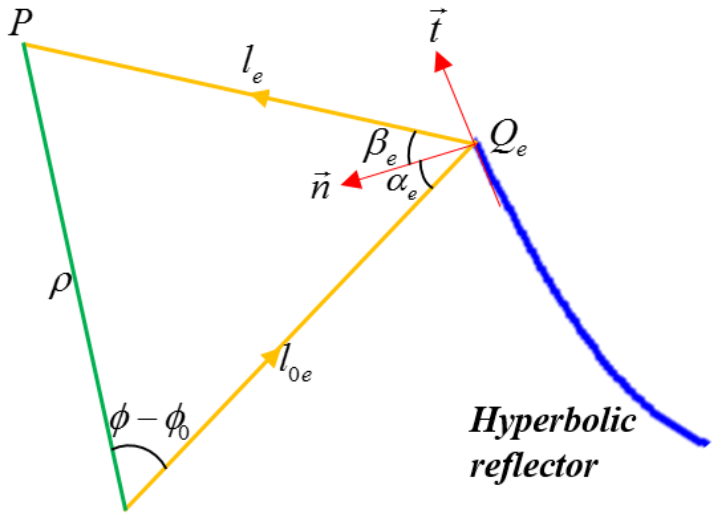

Figure 11 Edge diffraction geometry of the hyperbolic reflector

Figure 11 shows the edge diffraction geometry of the hyperbolic reflector where ϕ_0 is the edge boundary angle of the reflector since the reflector is placed between the angles of $[-\phi_0, \phi_0]$. α_e and β_e are the edge angles of incidence and reflection, respectively. l_{0e} and l_e are the edge diffraction parameters which are related with $\rho'(\phi_0)$ and $R(\phi_0)$, respectively. After the evaluation of the general equation of the edge point technique, the edge diffracted fields can be evaluated. The edge diffraction will be represented by E_d which can be written as

$$E_d = \frac{1}{jk}\frac{f(-\phi_0)}{g'(-\phi_0)}e^{-jkg(-\phi_0)} - \frac{1}{jk}\frac{f(\phi_0)}{g'(\phi_0)}e^{-jkg(\phi_0)} \tag{4.126}$$

where $f(-\phi_0)$ can be written as

$$f(-\phi_0) = -E_0\frac{e^{j\frac{\pi}{4}}}{\sqrt{2\pi}}\left[\cos\left(\frac{\alpha_e+\beta_e}{2}\right) - \sin\left(\frac{\alpha_e-\beta_e}{2}\right)\right]\frac{1}{\cos\alpha}\frac{\sqrt{\rho'(-\phi_0)}}{\sqrt{R(-\phi_0)}}. \tag{4.127}$$

By using Eq. (4.58), the inverse of the first derivative of the phase function can be obtained as

$$\frac{1}{g'(\phi')} = \frac{1}{2\rho'}\frac{\cos\alpha}{\cos\left(\frac{\beta+\alpha}{2}\right)\sin\left(\frac{\alpha-\beta}{2}\right)}, \tag{4.128}$$

which can be divided into two parts of reflection and transmission by the method of partial fraction that can be used as

$$\frac{\cos\alpha}{\cos\left(\frac{\beta+\alpha}{2}\right)\sin\left(\frac{\alpha-\beta}{2}\right)}=\frac{A}{\cos\left(\frac{\beta+\alpha}{2}\right)}+\frac{B}{\sin\left(\frac{\alpha-\beta}{2}\right)} \tag{4.129}$$

where the denuminators can be equated as

$$\frac{\cos\alpha}{\cos\left(\frac{\alpha+\beta}{2}\right)\sin\left(\frac{\alpha-\beta}{2}\right)}=\frac{A\sin\left(\frac{\alpha-\beta}{2}\right)+B\cos\left(\frac{\alpha+\beta}{2}\right)}{\cos\left(\frac{\alpha+\beta}{2}\right)\sin\left(\frac{\alpha-\beta}{2}\right)}, \tag{4.130}$$

which can be simplified as

$$\cos\alpha=\mathrm{A}\sin\left(\frac{\alpha-\beta}{2}\right)+\mathrm{B}\cos\left(\frac{\alpha+\beta}{2}\right) \tag{4.131}$$

So as to find the values of A and B, some logical values can be inserted instead of α or β. If α is inserted instead of β in Eq. (4.131), the value of B can be found as

$$B=1. \tag{4.132}$$

If the term $(\pi-\alpha)$ is inserted instead of β in Eq. (4.131), the value of A can also be found as

$$A=-1. \tag{4.133}$$

After the evaluations of A and B, Eq. (4.158) can be rewritten as

$$\frac{\cos\alpha}{\cos\left(\frac{\alpha+\beta}{2}\right)\sin\left(\frac{\alpha-\beta}{2}\right)}=\frac{1}{\sin\left(\frac{\alpha-\beta}{2}\right)}-\frac{1}{\cos\left(\frac{\alpha+\beta}{2}\right)}. \tag{4.134}$$

Finally, the inverse of the first derivative of the phase function can be obtained as

$$\frac{1}{g'(\phi')}=\frac{1}{2\rho'}\left[\frac{1}{\sin\left(\frac{\alpha-\beta}{2}\right)}-\frac{1}{\cos\left(\frac{\beta+\alpha}{2}\right)}\right]. \tag{4.135}$$

By using Eq. (4.135), the generalization of the edge diffraction coefficient $D(\phi_0)$ can be expressed as

$$D(\phi_0)=-\frac{e^{-j\frac{\pi}{4}}}{2\sqrt{2\pi}}\left[\frac{1}{\sin\left(\frac{\alpha_e-\beta_e}{2}\right)}-\frac{1}{\cos\left(\frac{\beta_e+\alpha_e}{2}\right)}\right]. \tag{4.136}$$

As a result, the result of nonuniform edge diffraction can be expressed as

$$E_d = E_0 \frac{e^{-jk(l_{0e}+l_e)}}{k\sqrt{l_{0e}l_e}}\left[D(-\phi_0)-D(\phi_0)\right] \tag{4.137}$$

where the edge diffraction parameters l_{0e} and l_e are are related with $\rho'(\phi_0)$ and $R(\phi_0)$ respectively. The edge diffraction parameters l_{0e}, l_e, α_e and β_e can be written as

$$l_{0e} = \frac{a\left(e^2-1\right)}{e\cos\phi_0 - 1}, \tag{4.138}$$

$$l_e = \sqrt{\rho^2 + l_{0e}^2 - 2\rho l_{0e}\cos\left(\phi-\phi_0\right)}, \tag{4.139}$$

$$\alpha_e = \cos^{-1}\frac{e\cos\phi_0 - 1}{\sqrt{e^2+1-2e\cos\phi_0}} \tag{4.140}$$

and

$$\beta_e = \sin^{-1}\frac{\rho\sin\left(\phi-\phi_0\right)}{l_e} - \alpha_e \tag{4.141}$$

respectively.

4.4.2 Uniform Diffracted Fields

The uniform diffracted fields consist of the reflected diffracted field and incident diffracted field. These uniform fields can be obtained from the nonuniform diffracted fields by using the method of the uniform theory of diffraction. The uniform fields will be evaluated for both the upper edge point and lower edge point of the reflector.

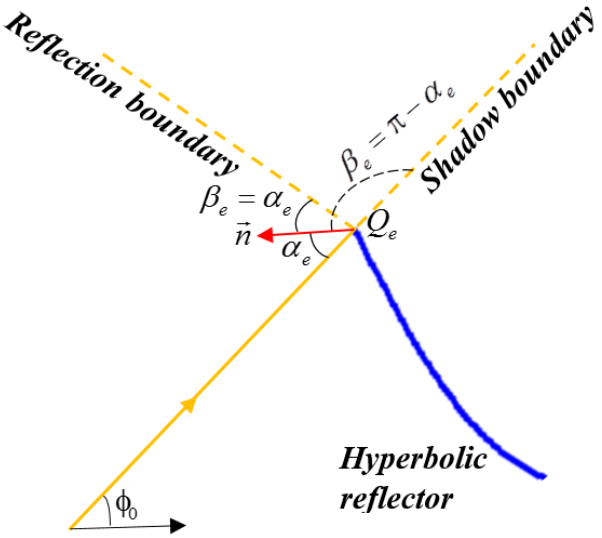

Figure 12 Geometrical places of the poles

Figure 12 shows the geometrical places of the poles at the edge point where α_e and β_e are the incident edge angle and the boundaries of reflection and shadow, respectively. The reflection and shadow boundaries can be found from the general diffraction coefficient given in the Eq. (4.136). The reflection boundary can be found by

$$\sin\left(\frac{\beta_e - \alpha_e}{2}\right) = 0. \tag{4.142}$$

Then the pole of the reflected diffracted field can be expressed as

$$\beta_e = \alpha_e. \tag{4.143}$$

The shadow boundary can be found by

$$\cos\left(\frac{\beta_e + \alpha_e}{2}\right) = 0. \tag{4.144}$$

Then the pole of the incident diffracted field can be evaluated as

$$\beta_e = \pi - \alpha_e. \tag{4.145}$$

It can also be seen that Eq. (4.137) approaches to infinity at β_e values found in Eq. (4.143) and Eq. (4.145). Consequently, the fields are named as nonuniform fields. As a consequence, the uniform fields should be evaluated.

4.4.2.1 Uniform Reflected Diffracted Field

The uniform reflected diffracted field can be derived from the nonuniform reflected diffracted field expression that can be defined as

$$D_r^{nu} = \frac{e^{-j\frac{\pi}{4}}}{k\sqrt{2}\left(2\sqrt{\pi}\right)} \frac{1}{\sin\left(\frac{\beta_e - \alpha_e}{2}\right)} \frac{e^{-jk(l_{0e}+l_e)}}{\sqrt{l_{0e}}\sqrt{l_e}}, \tag{4.146}$$

which is named as the nonuniform field since it approaches to infinity when β_e is equal to α_e.

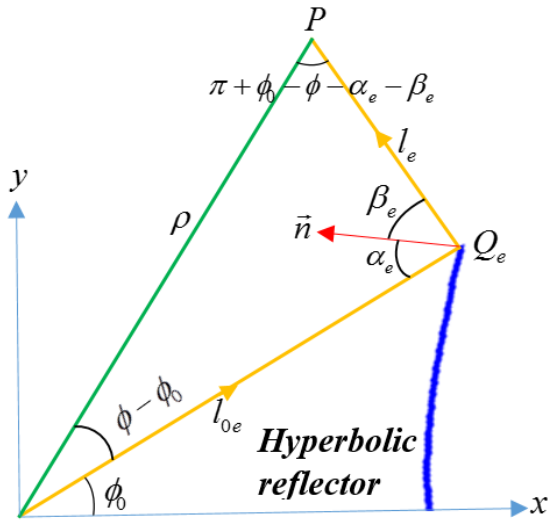

Figure 13 Upper edge point geometry of the hyperbolic reflector

Figure 13 shows the upper edge point geometry of the hyperbolic reflector at point Q_e where the parameters l_{0e} and l_e are the incident and scattered ray paths, respectively. α_e and β_e are the edge angles of incidence and reflection, respectively. ϕ_0 is the angle of upper boundary of the reflector. The uniform reflected diffracted field can be obtained by using the detour parameter ξ, signum function and Fresnel function. The detour parameter ξ can be defined as

$$\xi = -\sqrt{k\left(l_d - l_{GO}\right)} \tag{4.147}$$

where l_d is the sum of l_{0e} and l_e. l_{GO} is the sum of l_0 and l which are the incident and scattered ray paths of the GO. By using the detour parameter, Eq. (4.146) can be rearranged as

$$D_r^{nu} = \frac{e^{-j\frac{\pi}{4}}}{k\sqrt{2}\left(2\sqrt{\pi}\right)} \frac{1}{\sin\left(\frac{\beta_e-\alpha_e}{2}\right)} \frac{e^{-jk(l_{0e}+l_e)}}{\sqrt{l_{0e}}\sqrt{l_e}} \frac{e^{-j\xi^2}}{e^{-j\xi^2}} \frac{|\xi|}{|\xi|} \frac{\left|\sin\left(\frac{\beta_e-\alpha_e}{2}\right)\right|}{\left|\sin\left(\frac{\beta_e-\alpha_e}{2}\right)\right|} \tag{4.148}$$

where the square of ξ can be written as

$$\xi^2 = k\left(l_{0e} + l_e - l_0 - l\right). \tag{4.149}$$

Then Eq. (4.148) can be redefined as

$$D_r^{nu} = \frac{1}{\sqrt{2}} \frac{1}{\sin\left(\frac{\beta_e - \alpha_e}{2}\right)} \frac{e^{-jk(l_{0e}+l_e)}}{\sqrt{kl_{0e}}\sqrt{kl_e}} \frac{|\xi|}{e^{-j\xi^2}} \frac{\left|\sin\left(\frac{\beta_e - \alpha_e}{2}\right)\right|}{\left|\sin\left(\frac{\beta_e - \alpha_e}{2}\right)\right|} F\left[|\xi|\right] \tag{4.150}$$

where $F\left[|\xi|\right]$ is the Fresnel function that can be defined as

$$F\left[|\xi|\right] \approx \frac{e^{-j\frac{\pi}{4}}}{2\sqrt{\pi}} \frac{e^{-j\xi^2}}{|\xi|} \tag{4.151}$$

Finally, the uniform reflected diffracted field can be expressed as

$$D_r^{u} = \frac{1}{\sqrt{2}} F\left[|\xi|\right] \mathrm{sgn}\left(\sin\left(\frac{\beta_e - \alpha_e}{2}\right)\right) \frac{|\xi|}{\left|\sin\left(\frac{\beta_e - \alpha_e}{2}\right)\right|} \frac{1}{\sqrt{k}} \sqrt{\frac{l + l_0}{l_{0e} l_e}} \frac{e^{-jk(l_0+l)}}{\sqrt{kl_{0e}l_e}} \tag{4.152}$$

where β_e can be found by using the sine rule from Fig. 13. The sine rule can be defined as

$$\frac{l_e}{\sin(\phi - \phi_0)} = \frac{l_{0e}}{\sin(\pi + \phi_0 - \phi - \alpha_e - \beta_e)}. \tag{4.153}$$

Then β_e can be found as

$$\beta_e = \pi + \phi_0 - \phi - \alpha_e - \sin^{-1}\left(\frac{l_{0e}}{l_e}\sin(\phi - \phi_0)\right). \tag{4.154}$$

The other parameters of l_0, l, α_e, l_{0e} and l_e can be given as

$$l_0 = \frac{a\left(e^2 - 1\right)}{e\cos\phi_s - 1}, \tag{4.155}$$

$$l = \sqrt{\rho^2 + l_0^2 - 2\rho l_0 \cos(\phi - \phi_s)}, \tag{4.156}$$

$$\alpha_e = \cos^{-1}\frac{e\cos\phi_0 - 1}{\sqrt{e^2 + 1 - 2e\cos\phi_0}}, \tag{4.157}$$

$$l_{0e} = \frac{a\left(e^2 - 1\right)}{e\cos\phi_0 - 1} \tag{4.158}$$

and

$$l_e = \sqrt{\rho^2 + l_{0e}^2 - 2\rho l_{0e}\cos(\phi - \phi_0)} \tag{4.159}$$

respectively.

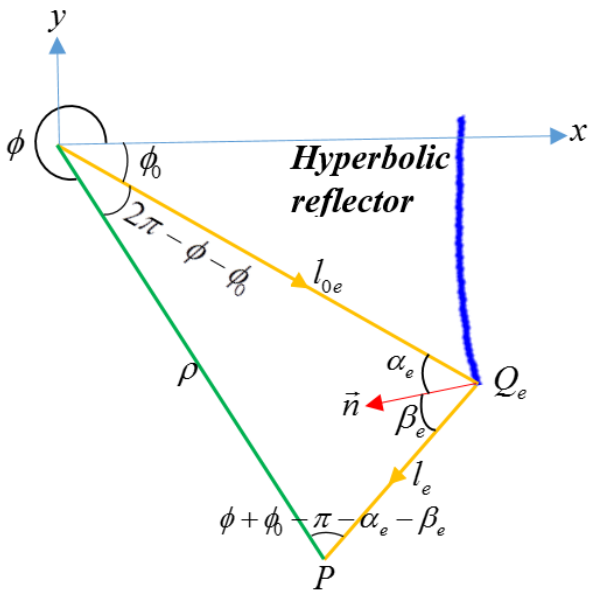

Figure 14 Lower edge point geometry of the hyperbolic reflector

Figure 14 shows the lower edge point geometry of the hyperbolic reflector at point Q_e where the parameter β_e should be redefined. The sine rule from Fig. 14 can also be used as

$$\frac{l_e}{\sin\left(2\pi-\phi-\phi_0\right)}=\frac{l_{0e}}{\sin\left(\phi+\phi_0-\pi-\alpha_e-\beta_e\right)}. \tag{4.160}$$

Then β_e can be found as

$$\beta_e=\phi+\phi_0-\pi-\alpha_e-\sin^{-1}\left(\frac{l_{0e}}{l_e}\sin\left(2\pi-\phi-\phi_0\right)\right). \tag{4.161}$$

Except l_e, the other parameters of l_0, l, α_e and l_{0e} in upper edge part are the same for the lower edge point. l_e can also be written as

$$l_e=\sqrt{\rho^2+l_{0e}^2-2\rho l_{0e}\cos\left(2\pi-\phi-\phi_0\right)}. \tag{4.162}$$

4.4.2.2 Uniform Incident Diffracted Field

In this part, the uniform reflected diffracted field can be obtained from the nonuniform incident diffracted field expression that can be defined as

$$D_i^{nu} = \frac{e^{-j\frac{\pi}{4}}}{k\sqrt{2}\left(2\sqrt{\pi}\right)} \frac{1}{\cos\left(\frac{\beta_e + \alpha_e}{2}\right)} \frac{e^{-jk(l_{0e}+l_e)}}{\sqrt{l_{0e}}\sqrt{l_e}}, \tag{4.163}$$

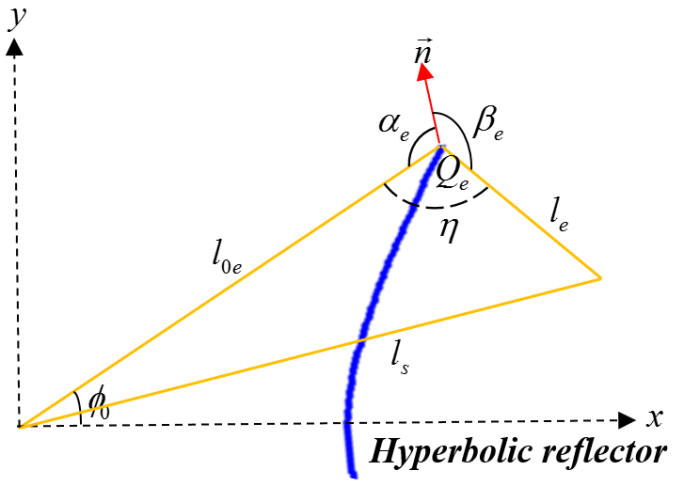

Figure 15 Geometry of the hyperbolic reflector for the incident diffraction

Figure 15 shows the incident diffraction geometry of the hyperbolic reflector at point Q_e where l_{0e} and l_e are the incident and scattered ray paths, respectively. l_s represents the sum of l_{0e} and l_e. α_e and β_e are the edge angles of incidence and reflection, respectively. By using detour parameter, Eq. (4.163) can be redefined as

$$D_i^{nu} = \frac{e^{-j\pi/4}}{k\sqrt{2}\left(2\sqrt{\pi}\right)} \frac{1}{\cos\left(\frac{\beta_e + \alpha_e}{2}\right)} \frac{e^{-jk(l_{0e}+l_e)}}{\sqrt{l_{0e}}\sqrt{l_e}} \frac{|\xi|}{|\xi|} \frac{\xi}{\xi} \tag{4.164}$$

where detour parameter can be defined as

$$\xi = -\sqrt{k\left(l_{0e} + l_e - l_s\right)}. \tag{4.165}$$

The square of the detour parameter can be expressed as

$$\xi^2 = k\left(l_{0e} + l_e - l_s\right). \tag{4.166}$$

By using Eq. (4.166), the diffraction equation can be redefined as

$$D_i^{nu} = \frac{e^{-j\frac{\pi}{4}}}{k\sqrt{2}\left(2\sqrt{\pi}\right)} \frac{1}{\cos\left(\frac{\beta_e + \alpha_e}{2}\right)} \frac{e^{-jk(l_s)}}{\sqrt{l_{0e}}} \frac{e^{-j\xi^2}}{\sqrt{l_e}} \frac{|\xi|}{|\xi|} \frac{\xi}{\xi}. \tag{4.167}$$

The equivalent of the detour parameter can be obtained by using the geometry given in Fig. 15. In order to evaluate it, the cosine rule can be used as

$$l_s^2 = l_e^2 + l_{0e}^2 - 2l_e l_{0e}\cos\eta \tag{4.168}$$

where η can be written as

$$\eta = 2\pi - \alpha_e - \beta_e. \tag{4.169}$$

Eq. (4.168) can be arranged as

$$\left(l_e + l_{0e}\right)^2 - l_s^2 = 2l_{0e}l_e\left(\cos\left(\alpha_e + \beta_e\right) + 1\right), \tag{4.170}$$

which can be rearranged as

$$4l_{0e}l_e\cos^2\left(\frac{\beta_e + \alpha_e}{2}\right) = \left(l_{0e} + l_e - l_s\right)\left(l_{0e} + l_e + l_s\right) \tag{4.171}$$

where the term $\left(l_{0e} + l_e - l_s\right)$ is equal to $\frac{\xi^2}{k}$. Then the detour parameter can be found as

$$\xi = -2\sqrt{\frac{kl_{0e}l_e}{l_{0e} + l_e + l_s}}\cos\left(\frac{\beta_e + \alpha_e}{2}\right). \tag{4.172}$$

By using Eq. (4.167), Eq. (4.167) can be restated as

$$D_i^{nu} = \frac{e^{-j\frac{\pi}{4}}}{k\sqrt{2}\left(2\sqrt{\pi}\right)}\frac{1}{cos\left(\frac{\beta_e + \alpha_e}{2}\right)}\frac{e^{-jkl_s}}{\sqrt{l_{0e}}}\frac{e^{-j\xi^2}}{\sqrt{l_e}}\frac{|\xi|}{\xi}\frac{-2\sqrt{\frac{kl_{0e}l_e}{l_{0e} + l_e + l_s}}\cos\left(\frac{\beta_e + \alpha_e}{2}\right)}{-2\sqrt{\frac{kl_{0e}l_e}{l_{0e} + l_e + l_s}}\cos\left(\frac{\beta_e + \alpha_e}{2}\right)} \tag{4.173}$$

where the Fresnel function $F\left[|\xi|\right]$ and the signum function can be used. After that, the uniform incident diffracted field can be written as

$$D_i^u = \mathrm{sgn}\left(\xi\right)F\left[|\xi|\right]\sqrt{\frac{2l_{0e}l_e}{k(l_{0e} + l_e + l_s)}}e^{-jkl_s} \tag{4.174}$$

where the parameters l_{0e}, l_e and β_e are also same as in the upper edge point of the reflected diffracted parameters. The value of β_e does not also change in lower edge point geometry.

The effects of both fields the incident diffracted and reflected diffracted will be analyzed in the part numerical analysis.

CHAPTER 5

NUMERICAL ANALYSIS

In this chapter, scattering process of the hyperbolic reflector will be examined in terms of reflection, transmission and uniform diffraction numerically. First of all, the results of the reflection integral of the modified theory of physical optics (MTPO) and physical optics (PO) will be compared numerically. Then, the MTPO integrals of reflected and transmitted fields will be analyzed. After that, the geometrical optics results obtained by the method of stationary phase will be investigated. Moreover, the uniform diffracted fields obtained by the method of uniform theory of diffraction (UTD) will be analyzed numerically. Furthermore, the summation of the reflected GO field and the uniform reflected diffracted fields will be analyzed and compared with the reflection integral of the MTPO. Finally, the summation of the incident field and the uniform incident diffracted field will be investigated in order to observe the fields in the luminous area.

Initially, the reflection integral of the MTPO and the integral of the reflected fields of the PO will be plotted and analyzed numerically. The reflection integral of the MTPO can be defined as

$$\vec{E}_{rs}^{MTPO} = -\vec{e}_z E_0 \frac{k e^{j\frac{\pi}{4}}}{\sqrt{2\pi}} \int_{-\phi_0}^{\phi_0} \cos\left(\frac{\beta+\alpha}{2}\right) \frac{e^{-jk\rho'}}{\sqrt{k\rho'}} \frac{e^{-jkR}}{\sqrt{kR}} \frac{\rho'}{\cos\alpha} d\phi'. \tag{5.1}$$

The integral of the reflected fields of the PO can be expressed as

$$\vec{E}_{rs}^{PO} = -\vec{e}_z E_0 \frac{k e^{j\frac{\pi}{4}}}{\sqrt{2\pi}} \int_{-\phi_0}^{\phi_0} \frac{e^{-jk\rho'}}{\sqrt{k\rho'}} \frac{e^{-jkR}}{\sqrt{kR}} \rho' d\phi'. \tag{5.2}$$

In order to investigate the reflection results of both MTPO and PO, the focal length and the observation distance ρ will respectively be taken as 1.5λ and 6λ where λ is the wavelength. The reflector is placed between the angles of $[-\phi_0, \phi_0]$.

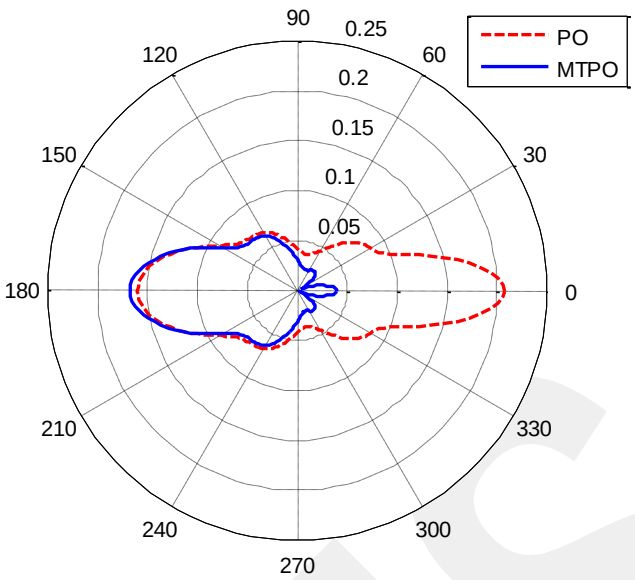

Figure 16 Reflected scattered fields by the hyperbolic reflector at $\phi_0 = 30^\circ$

Figure 16 shows the comparison of the reflected fields of MTPO and PO for a perfectly conducting hyperbolic reflector at $\phi_0 = 30^\circ$. It can be seen from Fig. 16 that the fields of MTPO and PO are in harmony between 90° and 270°. However, the PO integral deviates on a large scale between -90° and 90°. The reason is the construction of the PO integral [39]. Eq. (5.2) is not equal to zero for the stationary phase point at $\beta_s = \pi - \alpha_s$. For this reason, the PO integral includes the transmitted scattered fields as well.

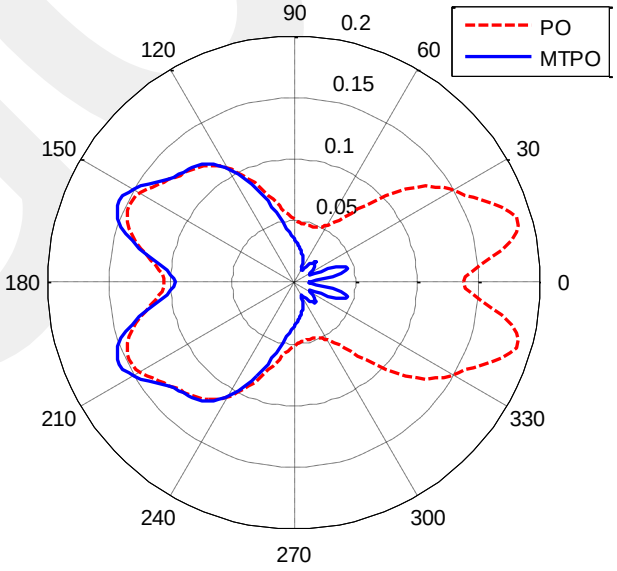

Figure 17 Reflected scattered fields by the hyperbolic reflector at $\phi_0 = 45^\circ$

Figure 17 shows the comparison of the reflection integrals of MTPO and PO at $\phi_0 = 45^\circ$. It can also be seen from Fig. 17 that the reflection integral of the PO also includes the transmitted scattered fields between the angles of -90° and 90°.

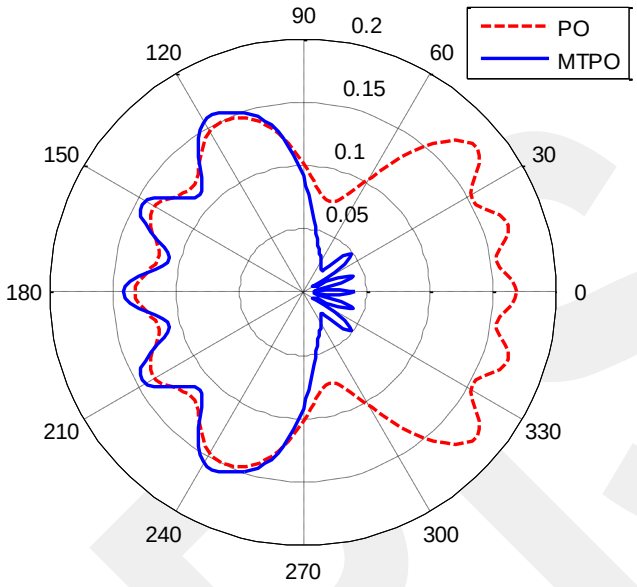

Figure 18 Reflected scattered fields by the hyperbolic reflector at $\phi_0 = 60^\circ$

Figure 18 depicts the comparison of the reflection integrals of MTPO and PO at $\phi_0 = 60^\circ$. The deviation of the PO integral between the angles of -90° and 90° can also be seen in Fig. 18.

Secondly, the reflected and the transmitted fields of the MTPO integral will be analyzed for the various reflector widths. For this analysis, the focal length and the observation distance will respectively be taken as 1.5λ and 6λ where λ is the wavelength.

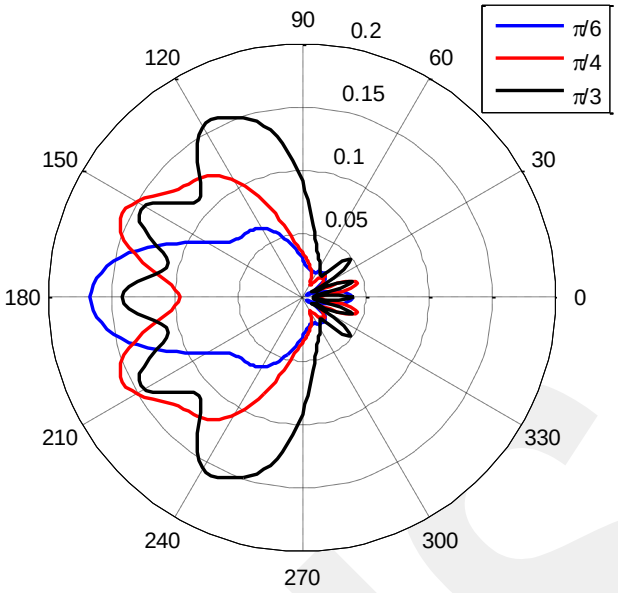

Figure 19 Reflected fields for several hyperbola widths

Figure 19 shows the reflected fields of the MTPO integral for several reflector widths. It can be seen that the reflection range increases as the reflector width increases. The reflector width having 60° has the largest reflection range among these three reflectors. Although the reflector width having 30° has the minimum reflection range, it has the greatest amplitude level at 180°.

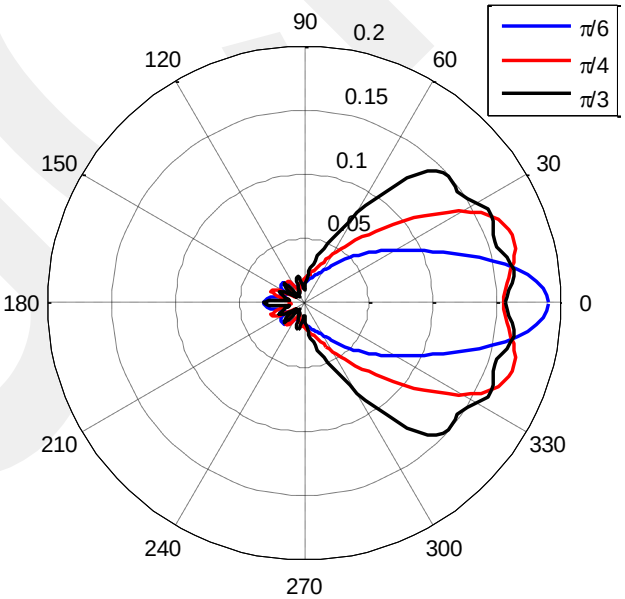

Figure 20 Transmitted fields for several hyperbola widths

Figure 20 shows the transmitted fields of the MTPO integral for several reflector widths. It can be seen from Fig. 20 that the transmission range increases as the reflector width increases. The reflector width having 60° has the largest transmission range among these three reflectors. Although the reflector width having 30° has the minimum transmission range, it shows the greatest amplitude level at 0°.

Thirdly, the reflected and the transmitted fields of the MTPO integral will be analyzed for different observation distances. For this analysis, the focal length will be taken as 1.5λ where λ is the wavelength.

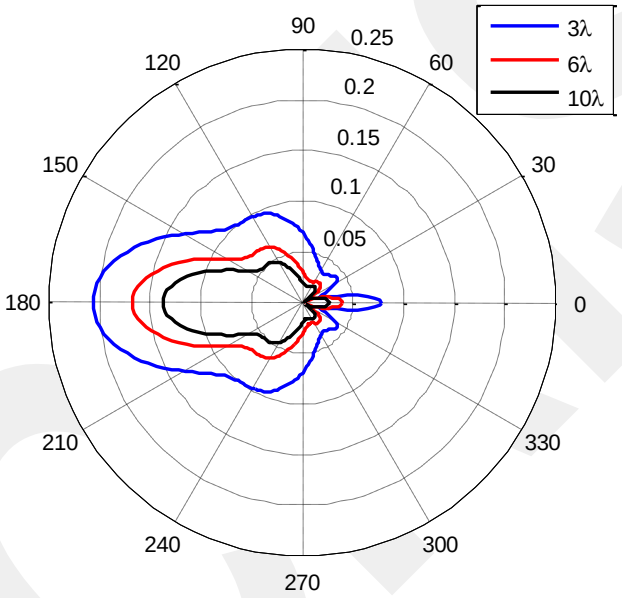

Figure 21 Reflected fields for different observation distances at $\phi_0 = 30^{\circ}$

Figure 21 depicts the reflected fields of the MTPO integral for different observation distances at $\phi_0 = 30^{\circ}$. It can be seen from Fig. 21 that the maximum amplitude level of the reflected fields decreases when the observation distance increases. In addition, the maximum amplitude level of the reflected fields can also be seen around 180°.

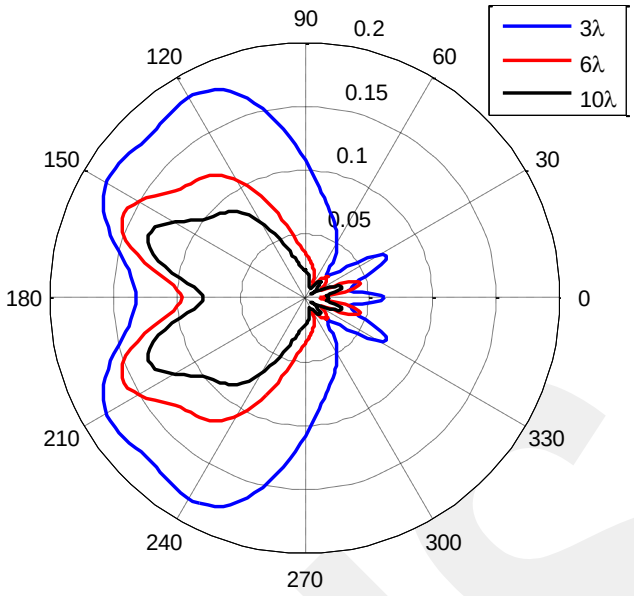

Figure 22 Reflected fields for different observation distances at $\phi_0 = 45^\circ$

Figure 22 shows the reflected fields of the MTPO integral for different observation distances at $\phi_0 = 45^\circ$. It can also be seen from Fig. 22 that the maximum amplitude level of the reflected fields decreases when the observation distance increases.

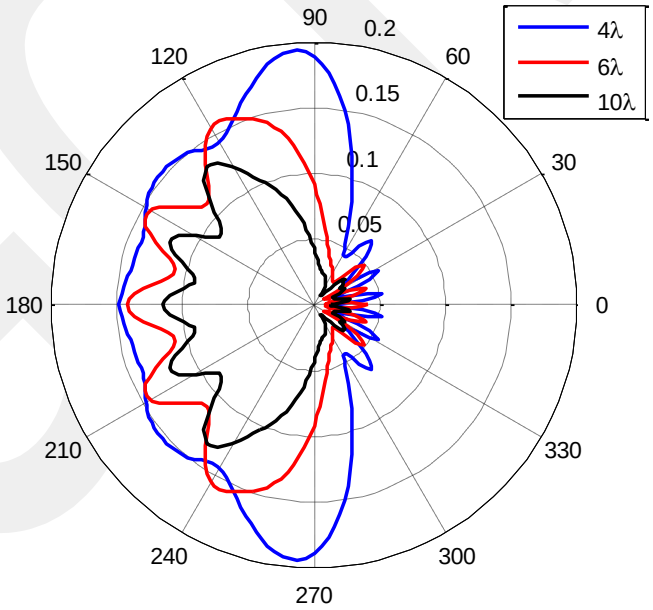

Figure 23 Reflected fields for different observation distances at $\phi_0 = 60^\circ$

Figure 23 shows the reflected fields of the MTPO integral for the different observation distances at $\phi_0 = 60^\circ$. It can be seen from Fig. 23 that the reflection ranges increase since the reflector widths increase. It can also be seen that the amplitude levels of the reflected fields decreases as the observation distance increases.

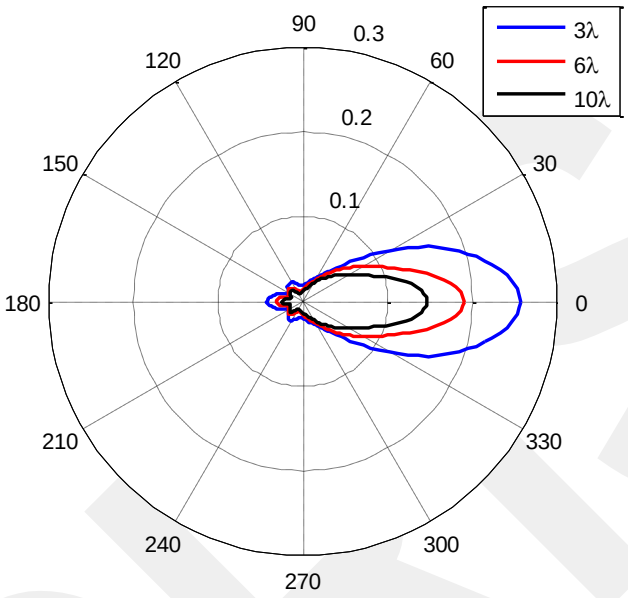

Figure 24 Transmitted fields for different observation distances at $\phi_0 = 30^\circ$

Figure 24 shows the transmitted fields for several observation distances at $\phi_0 = 30^\circ$. It can be seen from Fig. 24 that the maximum amplitude levels of the transmitted field decreases when the observation distance increases. The maximum amplitude level of the transmitted fields can be seen around 0°.

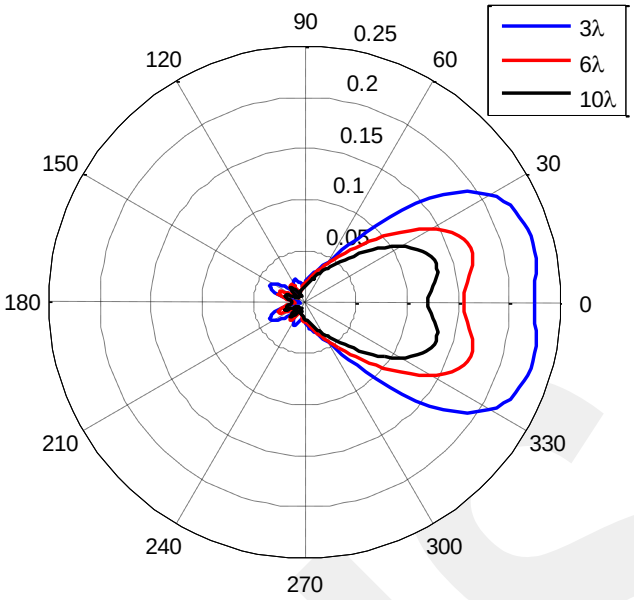

Figure 25 Transmitted fields for different observation distances at $\phi_0 = 45^\circ$

Figure 25 shows the transmittted fields for the different observation distances at $\phi_0 = 45^\circ$. It can also be seen from Fig. 25 that the maximum amplitude levels of the transmitted field decreases when the observation distance increases. The maximum amplitude level of the transmitted fields can also be seen around 0°.

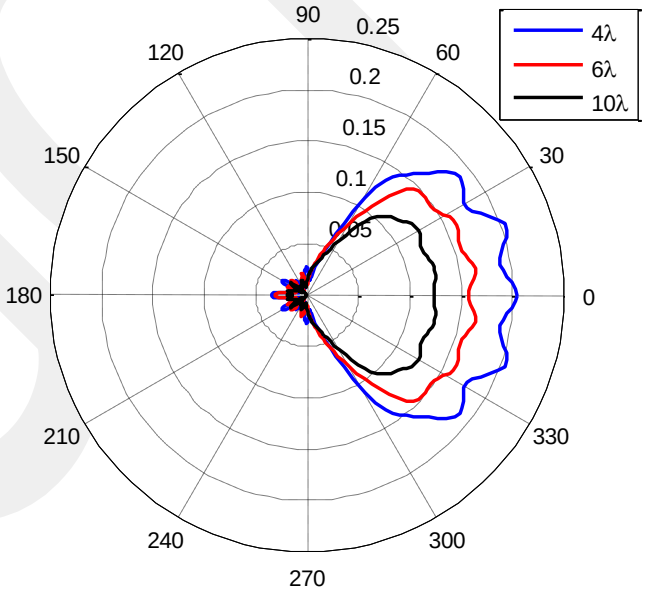

Figure 26 Transmitted fields for different observation distances at $\phi_0 = 60^\circ$

Figure 26 shows the transmittted fields for both the different observation distances at $\phi_0 = 60^\circ$. It can be seen from Fig. 26 that the transmission range increases since the reflector width increases, compared to Fig. 24 and Fig. 25. It can also be seen that the maximum amplitude levels of the transmitted field decreases when the observation distance increases. The maximum amplitude level of the transmitted fields can also be seen around 0°.

Fourthly, the geometrical optics (GO) results obtained by the method of stationary phase will be investigated numerically. The GO results will be analyzed for the various focal lengths of the various reflectors by changing of the center length a and the eccentricity e. The focal length of the hyperbolic reflector can be defined as

$$f = a(e+1) \tag{5.3}$$

where the variables a and e will be chosen to set the focal lengths as 1.5λ and 2λ, respectively. The observation distance will be taken as 6λ.

the variable a is chosen as 0.01 and the values of eccentricity e are chosen as 14 and 19 in order to set the focal lengths as 1.5λ and 2λ, respectively.

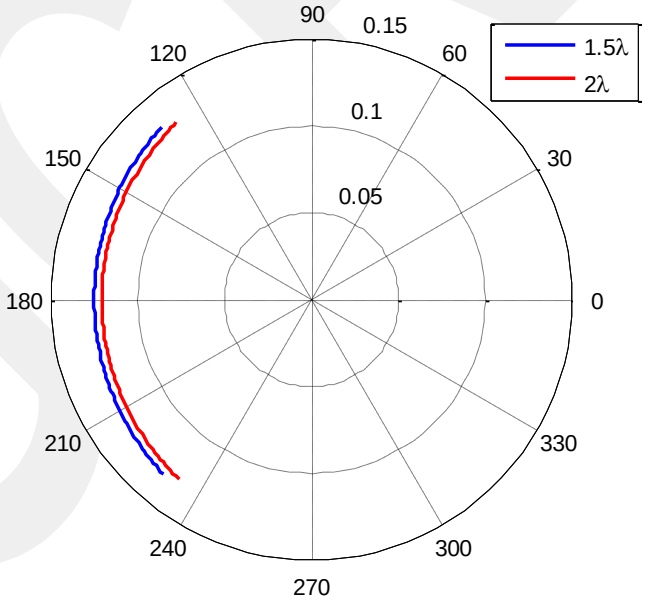

Figure 27 GO fields for different focal lengths with $a = 0.01$ at $\phi_0 = 30^\circ$

Figure 27 shows the geometrical optics (GO) fields for the various focal lengths at $\phi_0 = 30^\circ$ where the variable a is chosen as 0.01 and the values of eccentricity e are

chosen as 14 and 19 in order to set the focal lengths as 1.5λ and 2λ, respectively. It can be seen from Fig. 27 that the reflected fields varies almost between 125° and 235°.

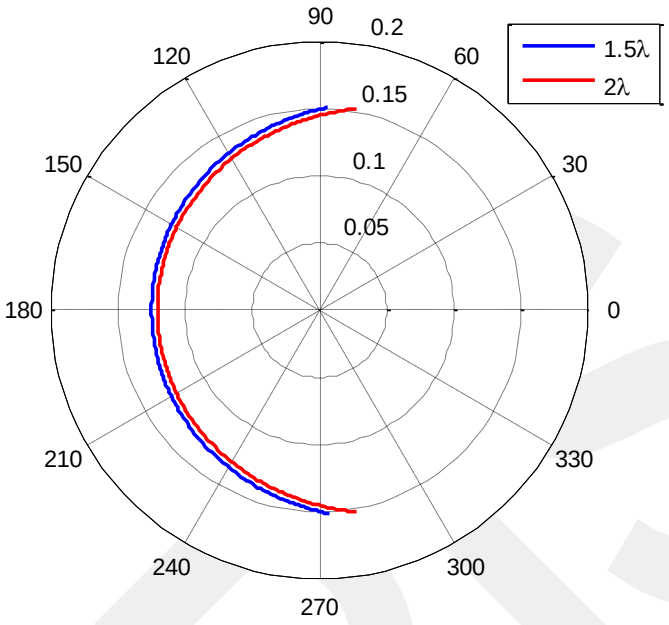

Figure 28 GO fields for different focal lengths with $a = 0.01$ at $\phi_0 = 60^{\circ}$

Figure 28 shows the geometric optics (GO) field for the various focal lengths at $\phi_0 = 60^{\circ}$ where the variable a is also chosen as 0.01 and the values of eccentricity e are also chosen as 14 and 19. It can be seen from Fig. 28 that the reflected fields deviates on a larger scale than the fields in Fig. 27 since the reflector width has increased.

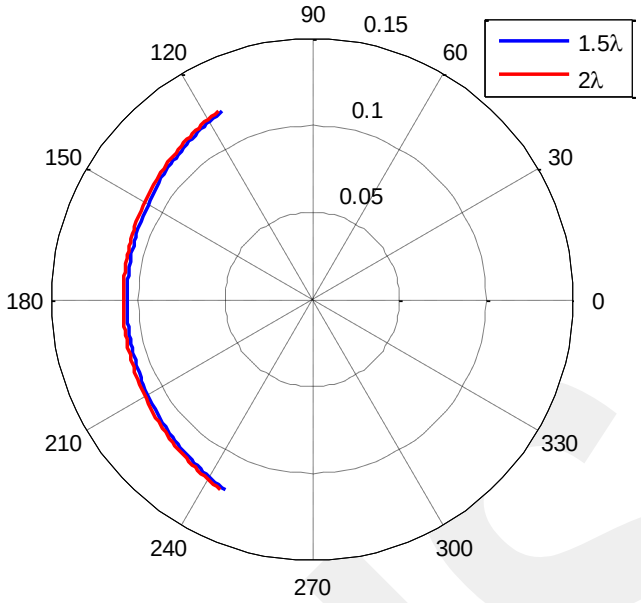

Figure 29 GO fields for different focal lengths with $a = 0.03$ at $\phi_0 = 30^\circ$

Figure 29 shows the geometric optics (GO) field for the various focal lengths at $\phi_0 = 30^\circ$ where the variable a is chosen as 0.03 and the values of eccentricity e are chosen as 4 and 5.67 in order to set the focal lengths as 1.5λ and 2λ, respectively. It can be seen from Fig. 29 that the reflected field varies almost between 120° and 240°.

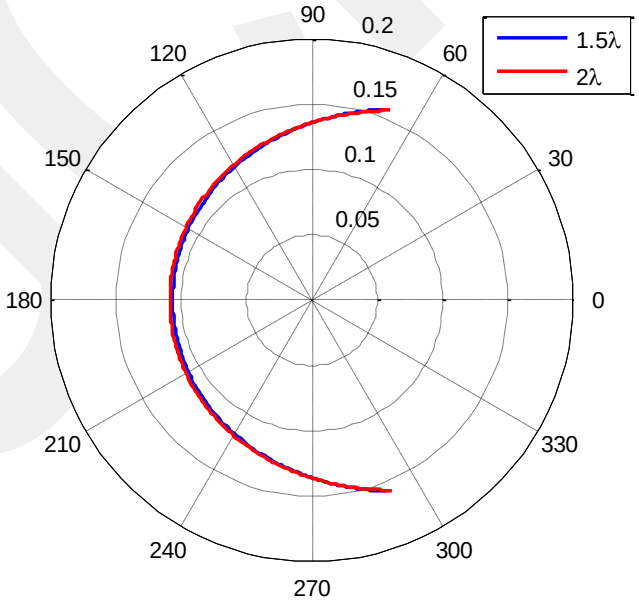

Figure 30 GO fields for different focal lengths with $a = 0.03$ at $\phi_0 = 60^\circ$

Figure 30 shows the geometric optics (GO) field for the various focal lengths $\phi_0 = 60^\circ$ where the variable a is also chosen as 0.03 and the values of eccentricity e are also chosen as 4 and 5.67 in order to set the focal lengths as 1.5λ and 2λ, respectively. It can be seen from Fig. 30 that the reflected fields deviates on a larger scale than the fields in Fig. 29 since the reflector width has increased. In addition, the reflected field varies almost between 70° and 290°.

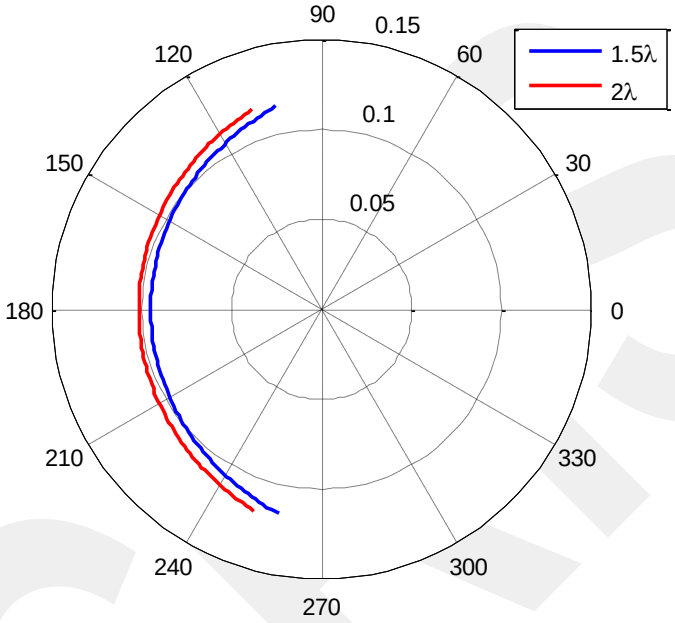

Figure 31 GO fields for different focal lengths with $a = 0.04$ at $\phi_0 = 30^\circ$

Figure 31 shows the geometric optics (GO) field for the various focal lengths at $\phi_0 = 30^\circ$ where the variable a is chosen as 0.04 and the values of eccentricity e are chosen as 2.75 and 4 in order to set the focal lengths as 1.5λ and 2λ, respectively. It can be seen from the Fig. 31 that the reflected field varies almost between the degrees of 110° and 250°.

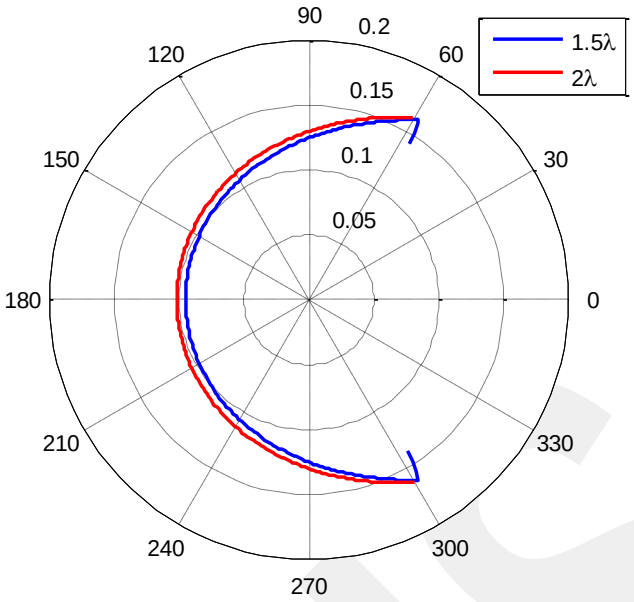

Figure 32 GO fields for different focal lengths with $a = 0.04$ at $\phi_0 = 60^\circ$

Figure 32 shows the geometric optics (GO) field for the various focal lengths for the refletor width at 60° where the variable a is also chosen as 0.04 and the values of eccentricity e are also chosen as 2.75 and 4 in order to set the focal lengths as 1.5λ and 2λ, respectively. It can be seen from Fig. 32 that the reflected fields deviates on a larger scale than the fields in Fig. 31 since the reflector width has increased.

In the next step, the uniform diffracted fields obtained by the method of the uniform theory of diffraction (UTD) will be investigated numerically. The uniform diffraction consists of the uniform reflected diffracted fields and uniform incident diffracted fields. The focal length and the observation distance will be chosen as 1.5λ and 6λ, respectively.

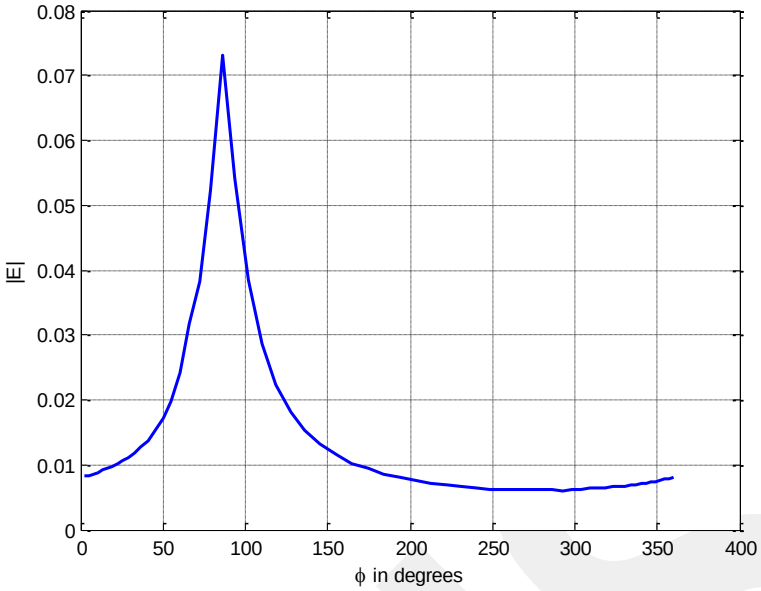

Figure 33 Uniform reflected diffracted field for the upper edge point at $\phi_0 = 60^\circ$

Figure 33 shows the uniform reflected diffracted field for the upper edge point of the reflector at $\phi_0 = 60^\circ$. The reflection boundary angle ϕ_e can be defined as

$$\phi_e = \pi + \phi_0 - 2\alpha_e - \sin^{-1}\left(\frac{l_{0e}}{\rho}\sin(2\alpha_e)\right) \tag{5.4}$$

where ϕ_e can be found as 87°. It can be seen from Fig. 33 that the peak value is in harmony with the reflection boundary ϕ_e.

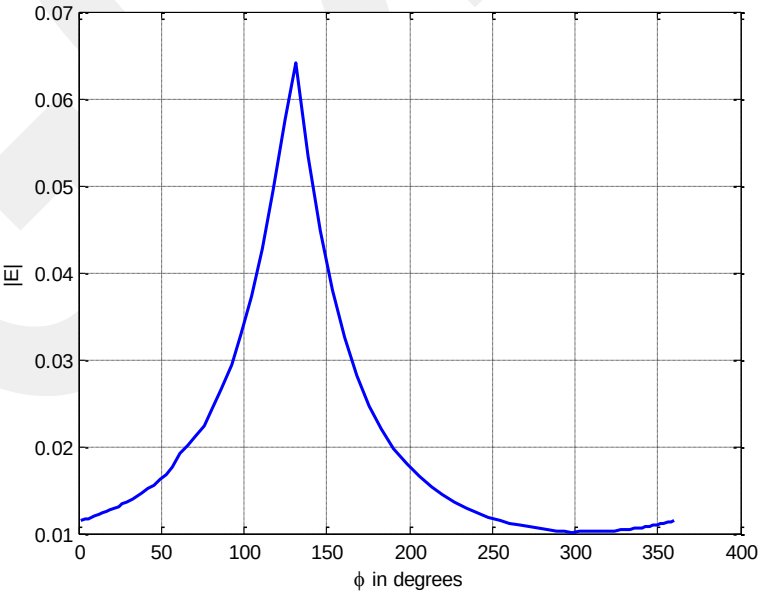

Figure 34 Uniform reflected diffracted field for the upper edge point at $\phi_0 = 30^\circ$

Figure 34 shows the uniform reflected diffracted field for the upper edge point of the reflector at $\phi_0 = 30^\circ$. By using Eq. (5.4), the reflection boundary angle ϕ_e can be found as 130°. It can also be seen from Fig. 34 that the peak value is in harmony with ϕ_e.

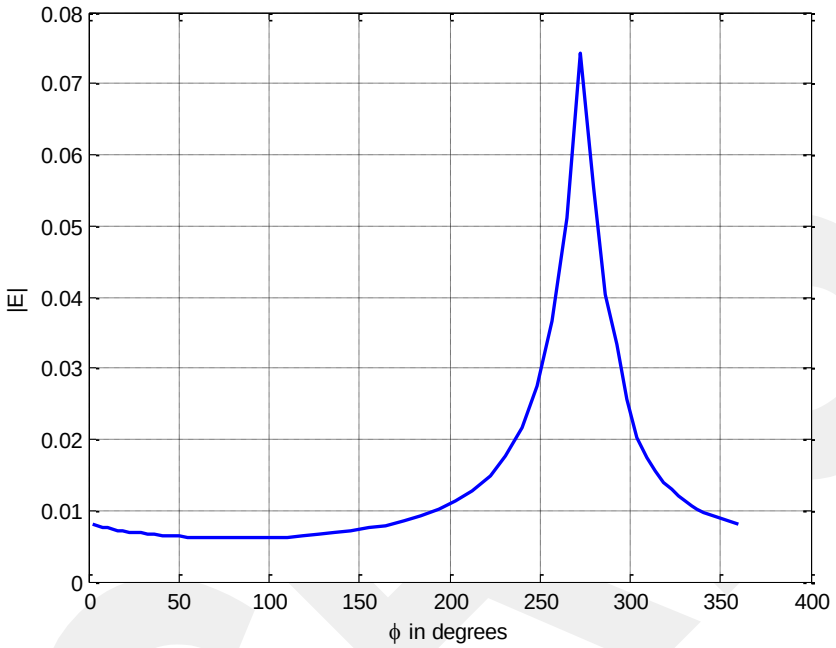

Figure 35 Uniform reflected diffracted field for the lower edge point at $\phi_0 = 60^\circ$

Figure 35 shows the uniform reflected diffracted field for the lower edge point of the reflector at $\phi_0 = 60^\circ$. The reflection boundary angle ϕ_e can be defined as

$$\phi_e = \pi - \phi_0 + 2\alpha_e + \sin^{-1}\left(\frac{l_{0e}}{\rho}\sin(2\alpha_e)\right) \tag{5.5}$$

where ϕ_e can be found as 274°. It can be seen from Fig. 35 that the peak value is in harmony with the reflection boundary ϕ_e.

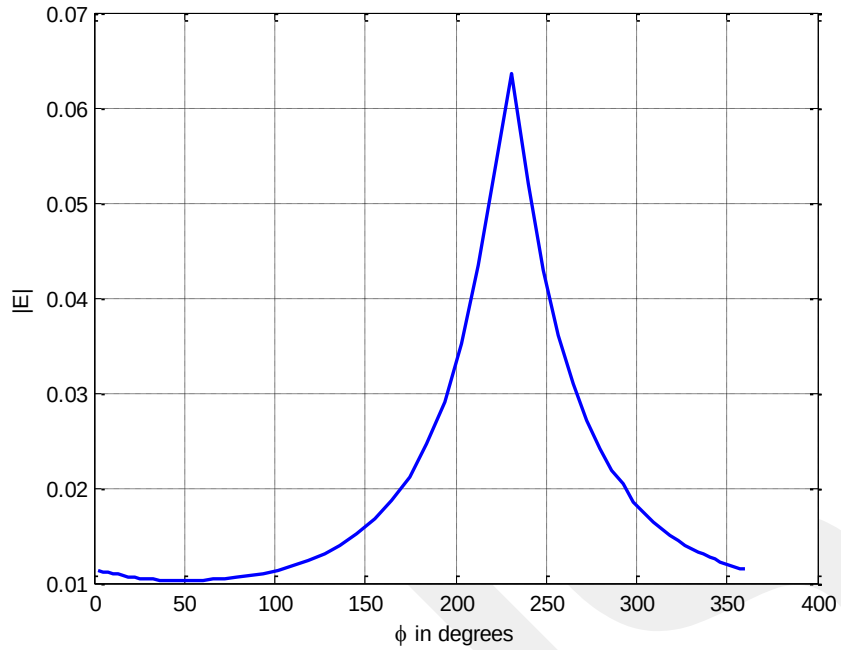

Figure 36 Uniform reflected diffracted field for the lower edge point at $\phi_0 = 30^\circ$

Figure 36 shows the uniform reflected diffracted field for the lower edge point of the reflector at $\phi_0 = 30^\circ$. By using the Eq. (5.5), the reflection boundary angle ϕ_e can be found as 230°. It can also be seen from Fig. 36 that the peak value is also in harmony with ϕ_e.

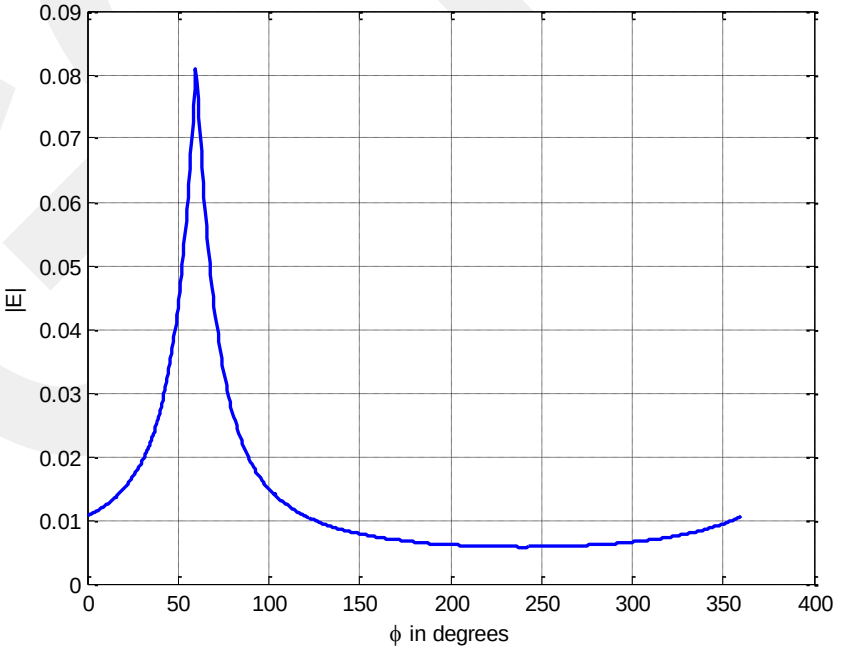

Figure 37 Uniform incident diffracted field for the upper edge point at $\phi_0 = 60^\circ$

Figure 37 shows the uniform incident diffracted field for the upper edge point of the reflector at $\phi_0 = 60^\circ$. The shadow boundary angle ϕ_e can be written as

$$\phi_e = \phi_0 \tag{5.6}$$

where ϕ_e is equal to 60° since the reflector width ϕ_0 is equal to 60°. It can be seen from Fig. 37 that the peak value is in harmony with the shadow boundary angle ϕ_e.

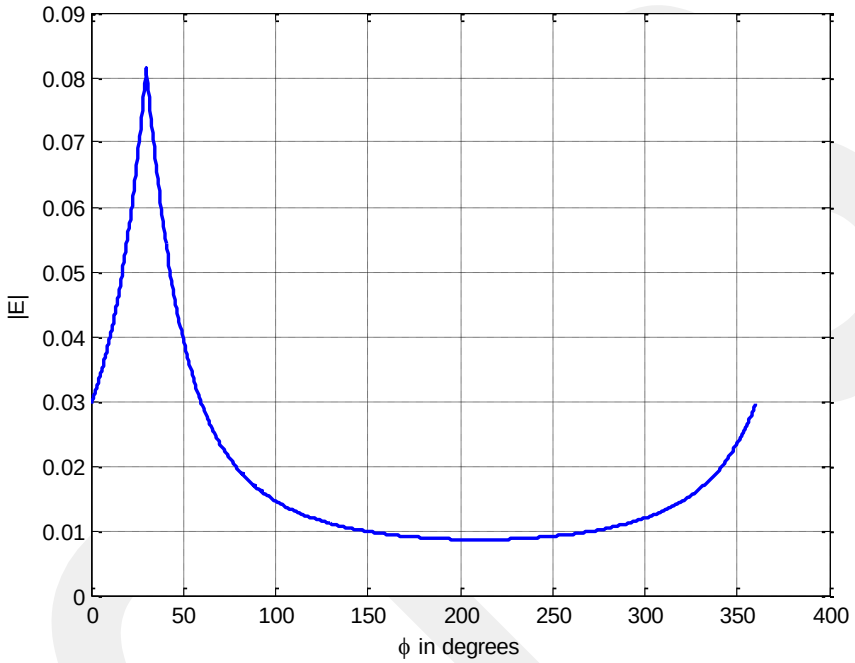

Figure 38 Uniform incident diffracted field for the upper edge point at $\phi_0 = 30^\circ$

Figure 38 shows the uniform incident diffracted field for the upper edge point of the reflector at $\phi_0 = 30^\circ$. By using Eq. (5.6), the shadow boundary angle ϕ_e can be found as 30°. It can also be seen from Fig. 38 that the peak value is also in harmony with ϕ_e.

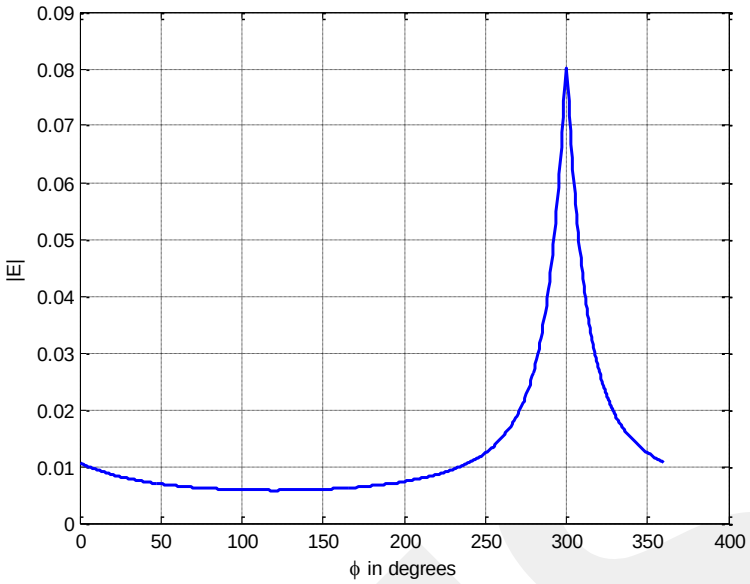

Figure 39 Uniform incident diffracted field for the lower edge point at $\phi_0 = 60^\circ$

Figure 39 shows the uniform incident diffracted field for the lower edge point of the reflector at $\phi_0 = 60^\circ$. The shadow boundary angle ϕ_e can be written as

$$\phi_e = 2\pi - \phi_0 \tag{5.7}$$

where ϕ_e can be found as 300°. It can be seen from Fig. 39 that the peak value is in harmony with the shadow boundary ϕ_e.

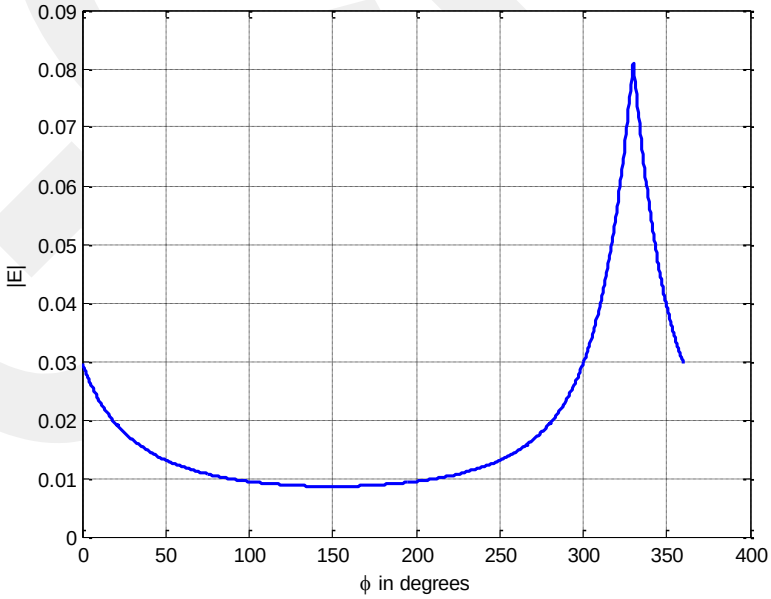

Figure 40 Uniform incident diffracted field for the lower edge point at $\phi_0 = 30^\circ$

Figure 40 shows the uniform incident diffracted field for the lower edge point of the reflector at $\phi_0 = 30^\circ$. By using Eq. (5.7), the shadow boundary angle ϕ_e can be found as 330°. It can also be seen from Fig. 40 that the peak value is also in harmony with ϕ_e.

In this section, the summation of the reflected GO field given in Eq. (4.117) and the uniform reflected diffracted fields given in Eq. (4.152) will be analyzed and compared with the reflection integral of the MTPO. For this analysis, the focal length and the observation distance will be chosen as 1.5λ and 6λ, respectively.

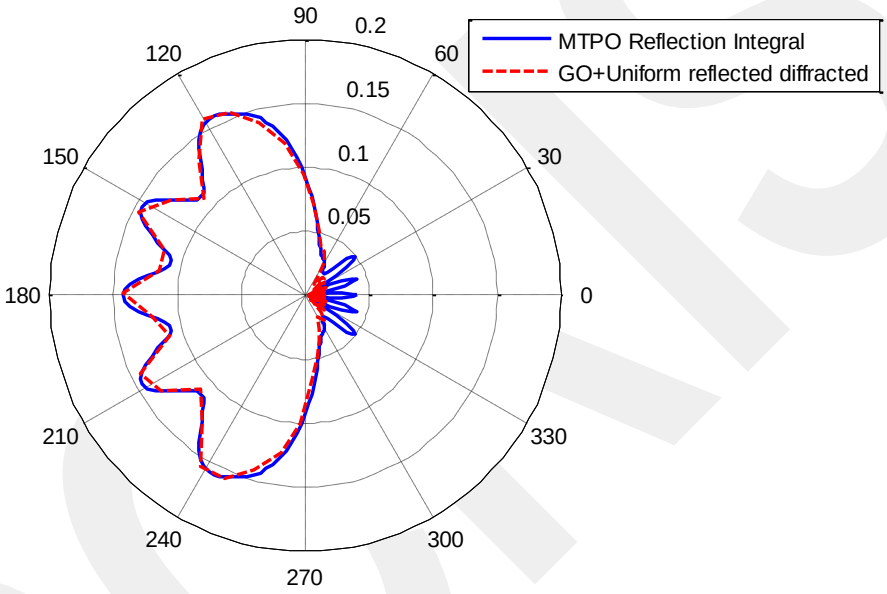

Figure 41 Comparison of the reflection integral of MTPO and the summation of the GO result and the uniform reflected diffracted fields at $\phi_0 = 60^\circ$

Figure 41 shows the comparison of the reflection integral of the MTPO as well as the summation of the fields of GO and the uniform reflected diffracted for the reflector at $\phi_0 = 60^\circ$. It can be seen from Fig. 41 that the summation of the GO result and the uniform reflected diffracted fields are in harmony with the reflection integral result of the MTPO.

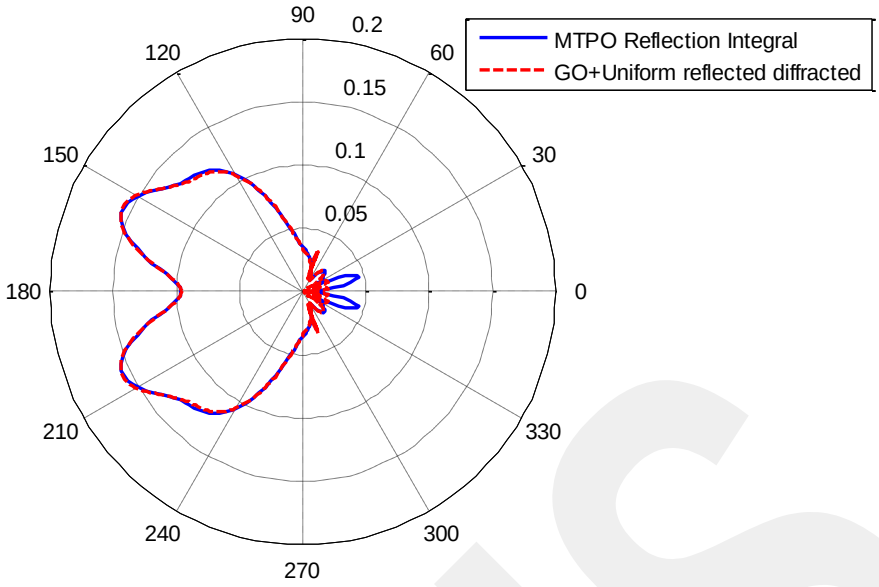

Figure 42 Comparison of the reflection integral of MTPO and the summation of the GO result and the uniform reflected diffracted fields at $\phi_0 = 45^\circ$

Figure 42 also shows the comparison of the reflection integral of the MTPO as well as the summation of the fields of GO and the uniform reflected diffracted for the reflector at $\phi_0 = 45^\circ$. It can also be seen from Fig. 42 that the summation of the GO result and then uniform reflected diffracted fields are in harmony with the reflection integral result of the MTPO.

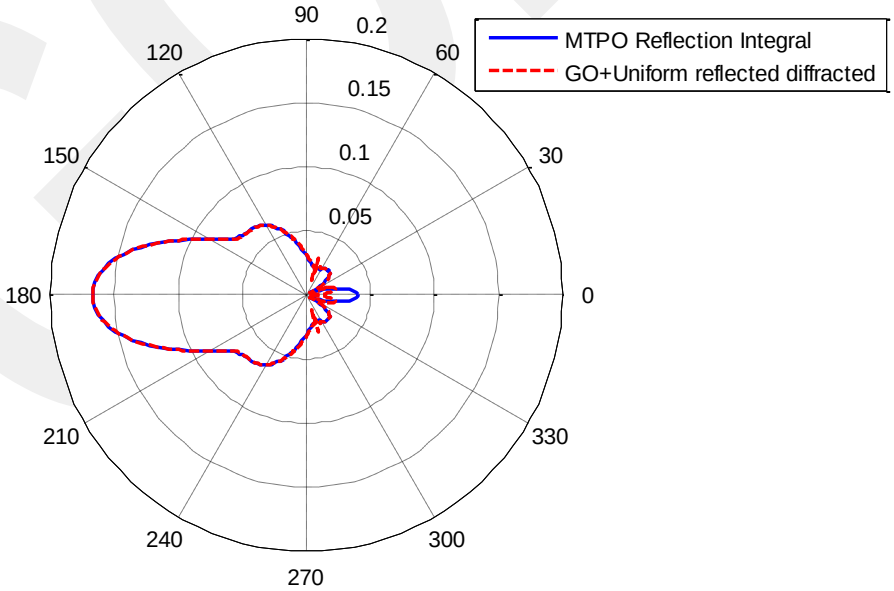

Figure 43 Comparison of the reflection integral of MTPO and the summation of the GO result and the uniform reflected diffracted fields at $\phi_0 = 30^\circ$

Figure 43 also shows the comparison of the reflection integral of the MTPO as well as the summation of the fields of GO and the uniform reflected diffracted for the reflector at $\phi_0 = 30^\circ$. It can be seen from Fig. 43 that the summation of the GO result and the uniform reflected diffracted fields are also in harmony with the reflection integral result of the MTPO.

Lastly, the summation of the incident field given in Eq. (4.10) and the uniform incident diffracted field given in Eq. (4.177) will be investigated in order to observe the fields in the luminous area. For this analysis, the focal length and the observation distance will be chosen as 1.5λ and 6λ, respectively.

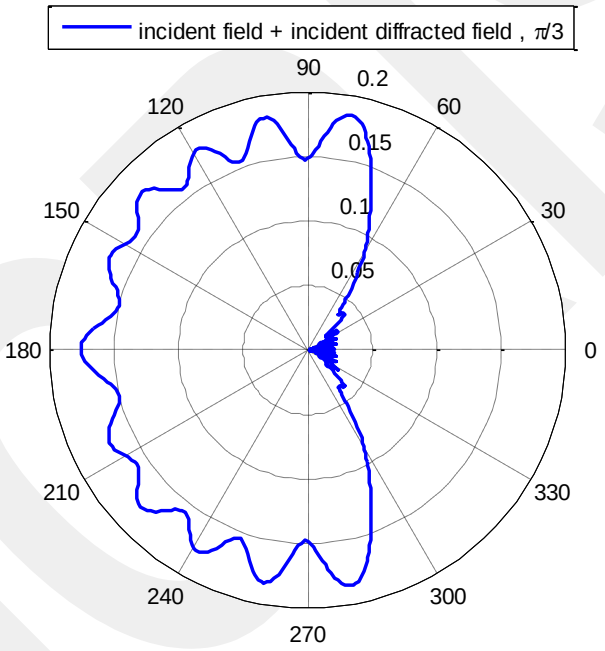

Figure 44 Summation of the incident field and the incident diffracted fields at $\phi_0 = 60^\circ$

Figure 44 shows the summation of the incident field and the uniform incident diffracted field for the reflector at $\phi_0 = 60^\circ$ in the luminous area. It can be seen from Fig. 44 that the summation of the incident field and the incident diffracted field varies between 60° and 300°.

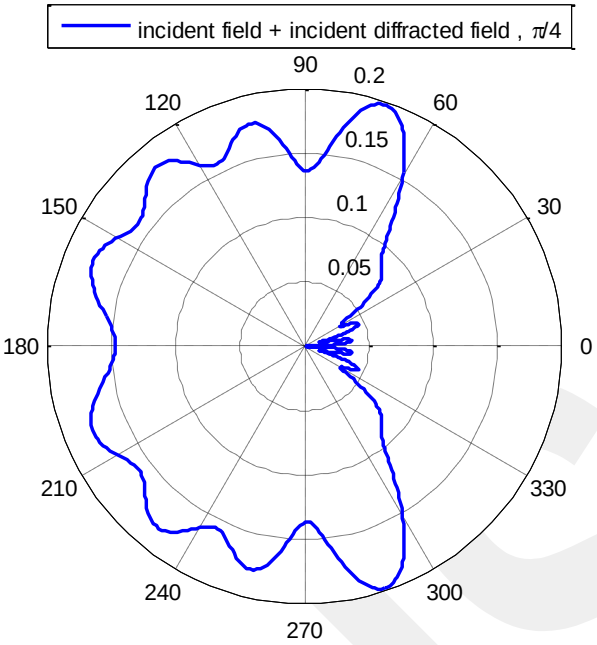

Figure 45 Summation of the incident field and the incident diffracted fields at $\phi_0 = 45^\circ$

Figure 45 shows the summation of the incident field and the uniform incident diffracted field for the reflector at $\phi_0 = 45^\circ$ in the luminous area. It can be seen from Fig. 45 that the summation of the incident field and the incident diffracted field varies between 45° and 315°.

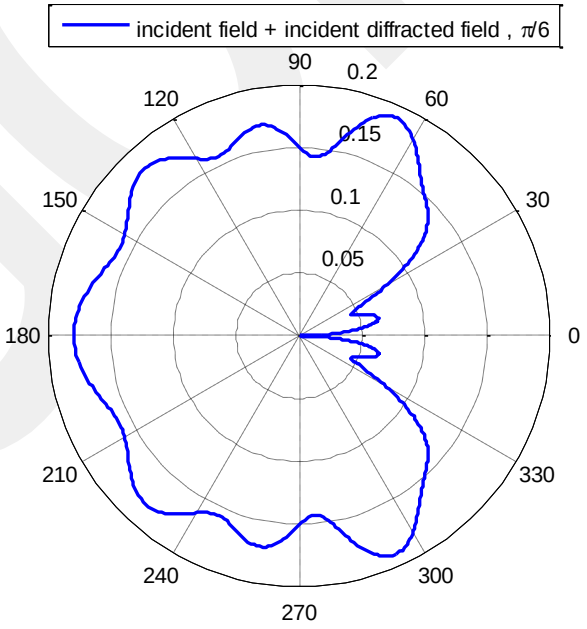

Figure 46 Summation of the incident field and the incident diffracted fields at $\phi_0 = 30^\circ$

Figure 46 shows the summation of the incident field and the uniform incident diffracted field for the reflector at $\phi_0 = 30^\circ$ in the luminous area. It can be seen from Fig. 46 that the summation of the incident field and the incident diffracted field varies between 30° and 330°. It can also be seen that the summation of these fields covers a wider range as the reflector width decreases.

CHAPTER 6

CONCLUSIONS

In this thesis, the scattering process through a convex hyperbolic reflector was investigated. The study was based mainly on the modified theory of physical optics (MTPO) suggested by Umul. The theory suggests the exact solution of the scattering fields, especially compared to the method of the classical physical optics (PO). The difference of MTPO comes from its axioms. The new unit vector expression, taking reflection angle as a variables of the integral and taking into consideration the perfectly conductor surface with its aperture part together construct the difference of MTPO.

Furthermore, in this study, in order to evaluate the scattering integral, the hyperbola geometry was firstly determined. Since a classical hyperbola has two focal points and two legs, the right leg (convex) of the hyperbola was preferred for this thesis and the focal point of the left leg of the hyperbola was chosen in order to illuminate this convex leg. The hyperbola geometry was so important for the definition of the incident ray path ρ' which is the key factor for the construction of the unit vector and the asymptotic evaluations of the scattering integral. After that, the stationary phase points were found using the method of stationary phase. One of them was related with the reflection and the other one was related with the transmission. Both stationary phase points were used in MTPO integrals in order to define the integrals of reflection and transmission, individually. After the definitions of integrals as in Ref. [37], the results of the reflected and transmitted fields of the MTPO integral were analyzed. Moreover, the integrals of the PO and MTPO were analyzed and compared numerically. It was seen that the MTPO individually offered information about both the reflected and transmitted fields. However, the reflection integral of the PO failed to offer information only about reflected fields. It included the transmitted fields in the reflection integral as well.

Besides, the geometrical optics (GO) fields and edge diffracted fields were obtained using the method of stationary phase and edge point technique, respectively. After the asymptotic evaluation of the edge point diffraction by the edge point technique, it was seen that the results were non-uniform since the diffraction result approaches to infinity at the transition regions. In order to obtain the uniform diffracted fields, the method of uniform theory of diffraction (UTD) was used. By using the UTD, the uniform reflected diffracted fields were found for both the upper and lower edge points, respectively. Then the uniform incident diffracted fields were found for both the upper and lower edge points, individually. After that, the GO results and the results of the uniform diffracted fields were numerically analyzed.

In addition, the summation of the results of the GO field and the uniform reflected diffracted field was analyzed numerically. After the analysis, it was seen that the summation of these fields was the same result as the reflection integral of the MTPO. Finally, the summation of the incident field and the uniform incident diffracted field was investigated and numerically analyzed for the several hyperbola reflector widths in order to observe the fields in the luminous area.

As a result, the scattering behavior of a hyperbolic reflector was gone over by mainly focusing on the modified theory of physical optics. The reflected fields, the transmitted fields, the GO fields, the nonuniform edge diffraction as well as the uniform reflected diffracted and uniform incident diffracted fields were investigated and numerically analyzed using the related methods in this thesis.

REFERENCES

1. **Franceschetti G. and Mohsen A., (1986),** "*Recent developments in the analysis of reflector antennas. A review*", IEE PROCEEDINGS, vol. 133, p. 65.

2. **Terados M. A. B., (1999),** "*Reflector Antennas*", Wiley Encyclopedia of Electrical and Electronics Engineering.

3. **Ramanujam P., Hoffmeister R., Kresco D., Park B.M., (1996),** "Different Methods of PO Analysis in a Dual Reflector Antenna With a Shaped Main Reflector", IEEE, vol. 1, p. 230.

4. **Floreani M.G., Zich R.E., Aulisio G., (2000),** "*Design and Experimental Validations of a New Shaped Subreflector Geometry for EMC Oriented Cassegrain System*", in Environmental Electromagnetics, CEEM 2000. Proceedings. Asia-Pacific Conference on, Shanghai, pp. 167-169, 1-3.

5. **Şafak M., (1989),** "*Radiation Pattern of an Offset Hyperbolic Reflector*", IEEE Transactions on Antennas and Propagation, vol. 37, no. 2, pp. 251-253.

6. **Farahat N., Mittra R.,Carrio´n J., Sanchez J., (2006),** "*Numerical analysis of large reflector system used as a ground station antenna*", in Aerospace Conference, 2006 IEEE, Big Sky, MT, pp. 1-15.

7. **Elkamchouchi, Y.H., Elkamchouchi, H.M., El-Khamy, S.E., (1998),** "*Analysis of parabolic and hyperbolic cylindrical reflector antennas using the method of moments*", Fifteenth National Radio Science Conference, Helwan, Cairo, Egypt, pp. B4/1 - B4/8.

8. **˘Skokic´ S. and Martini E., Maci S., (2005),** "*Radar-invisibility on axis of rotationally symmetric reflectors*", IEEE Antennas and Wireless Propagation Letters, vol. 4, pp. 1-4.

9. **Fomel S. and Kazinnik R., (2012),** "*Non-hyperbolic common reflection surface*", Geophysical Prospecting, vol. 61, pp. 21-27.

10. **Chou H. T. and Tuan S. C., (2013),** "*Analytic transient analysis of radiation from hyperboloid reflector antennas via surface curvature continuation of ellipsoidal surfaces*", Electronics Letters, vol. 49, no. 6, pp. 381-382.

11. **Mousavi, P., Shafai L., Veidt B., Dewdney P., (2001),** "*Feed-reflector design for large adaptive reflector antenna (LAR)*", IEEE Transactions on Antennas and Propagation, vol. 49, no. 8, pp. 1142 – 1154.

12. **Xiao L., Yang H., Liu X., Xu Q., Xiong X., (2010),** "*New type optical Cassegrain antenna with lenses telescope system*", International Journal for Light and Electron Optics, vol. 121, no. 6, pp. 521-525.

13. **Ma X., Yang H., Wang B., Jiang P., Yu M., Huang Y., Ke S., (2014),** "*An optimum structure design for Cassegrain optical system*", International Journal for Light and Electron Optics, vol. 125, no. 3, pp. 1423-1426.

14. **Chen Z., Yang H., Wang X., Wang J., Huang X., (2012**), "*Theoretical analysis and test for off-axis Cassegrain optical antenna*", International Journal for Light and Electron Optics, vol. 123, no. 3, pp. 268-271.

15. **Haeger T. A. and Lee J. J., (1990),** "*Comparisons Between a Shaped and Nonshaped Small Cassegrain Antenna*", IEEE Transactions on Antennas and Propagation, vol. 38, no. 12, pp. 1920-1924.

16. **Hakli' J., Ala-Laurinaho' J., Koskinen' T., Saily' J., Lonnqvist' A., Mallat' J., Tuovinen J., Raisanen' A. V., (2002),** "*Synthesis of a Dual Reflector Feed System for a Hologram CATR*", IEEE Antennas and Propagation Society International Symposium, vol. 4, pp. 580-583.

17. **Agrawal V. D. and Imbriale W. A., (1979),** "*Design of a Dichroic Cassegrain Subreflector*", IEEE Transactions on Antennas and Propagation, vol. 27, no. 4, pp. 466-473.

18. **Galindo V., Imbriale W. A., Mittra R., (1987),** "*On the theory of the synthesis of single and dual offset shaped reflector antennas*", IEEE Transactions on Antennas and Propagation, vol. 35, no. 8, pp. 887-896.

19. **Pippi A., Caruso A., Sabbadini M., Maci S., (2004),** "*The shadow boundary integral technique for cassegrain subreflectors*", IEEE Antennas and Propagation Society International Symposium, vol. 4, pp. 4188 – 4191.

20. **Armogida A., Pagana E., Stringhetti L., Volpi L., (2004),** "*Novel dual reflector antenna for surveillance radar*", Radar Conference, in EURAD 2004, First European, pp. 177-180.

21. **Tyo J. S., Farr E. G., Lawry D. I., (2005),** "*Effect of defocus on the prompt response of a reflector IRA*", IEEE Transactions on Antennas and Propagation, vol. 53, no. 10, pp. 3247-3254.

22. **Bozzi M., Formaggi M., Perregrini L., (2006),** "*Design of Dichroic Mirrors for Space Applications by the MoM/BI-RME Method: from Planar to Curved Structures*", Antennas and Propagation Society International Symposium 2006, IEEE, pp. 2455 – 2458.

23. **Kim Y. and Lee T. H., (2006),** "*An Approach of Shaping Offset Dual Reflector Antennas by Controlling Location of Caustic for Local Dual Reflector System*", Antennas and Propagation Society International Symposium 2006, IEEE, pp. 4405 – 4408.

24. **Jiang C., Li D., Zhou G., Luo H., (2011), "***Precision Forming Technology and Application for High-precision Sandwich Reflector Panels*", Electronic and Mechanical Engineering and Information Technology (EMEIT), 2011 International Conference on, vol. 3, pp. 1164 – 1168.

25. **Mirkamali A. and Laurin J. J., (2012),** "*A Novel Two Dimensional Circular Lens for Beam Steering Applications*", Antennas and Propagation Society International Symposium (APSURSI), 2012 IEEE, pp. 1-2.

26. **Mirkamali A., Laurin J. J., Siaka F., Deban R., (2013),** "*A Planar Lens Antenna With Circular Edge Inspired by Gaussian Optics*", IEEE Transactions on Antennas and Propagation, vol. 61, no. 9, pp. 4476-4483.

27. **Silver S., (1949),** "*Microwave Antenna Theory and Design*", McGraw-Hill, New York.

28. **Keller J. B., (1962),** "*Geometrical Theory of Diffraction*", Journal of the Optical Society of America, vol. 52, no. 2, pp.116-130.

29. **Kouyoumjian R. G. and Pathak P. H., (1974),** "*A Uniform Theory of Diffraction for Edge in A Perfectly Conducting Surface*", Proceedings of the IEEE, vol. 62, no. 11, pp. 1448-1461.

30. **McDonald H. M., (1913),** "*The Effect Produced by An Obstacle on A Train of Electric Waves*", Phil. Trans. R. Soc. Lond., Ser. A., Math. Phys. Sc., vol. 212, pp. 299-337.

31. **Ufimtsev P. Ya., (2007),** "*Fundamentals of The Physical Theory of Diffraction*", Wiley, New Jersey.

32. **Umul Y. Z., (2004),** "*Modified Theory of Physical Optics*", Optics Express vol. 12, no. 20, pp. 4959–4972.

33. **Ufimtsev, P., (2008),** "*New Insight into the Classical Macdonald Physical Optics Approximation*", IEEE Antennas and Propagation Magazine, vol. 50, no. 3, pp. 11-20.

34. **Stutzman W.L., Thiele G.A., (1998),** "*Antenna Theory and Design*", second ed., Wiley, New York.

35. **Ufimtsev, P., (2009),** "*Theory of Edge Diffraction in Electromagnetics: Origination and Validation of the Physical Theory of Diffraction*", Raleigh, NC, SciTech Publishing, Inc.

36. **James G. L., (1979),** "*Geometrical Theory of Diffraction for Electromagnetic Waves*", Peter Peregrinus Ltd. on behalf of Institution of Electrical Engineers, United Kingdom.

37. **Umul Y. Z., (2008),** "*Scattering of a line source by a cylindrical parabolic impedance surface*", Journal of the Optical Society of America, vol. 25, no. 7, pp. 1652-1559.

38. **Umul Y. Z., (2006),** "*Modified Theory of Physical Optics Solution of Impedance Half Plane Problem*", IEEE Antennas and Propagation, vol. 54, no. 7, pp. 2048-2053.

39. **Umul Y. Z., (2005),** "*Modified theory of physical optics approach to wedge diffraction problems*", Optics Express, vol. 13, no. 1, pp. 216-224.

APPENDICES

CURRICULUM VITAE

PERSONEL INFORMATION
Surname, Name: Çelik, Süleyman Burak
Date and Place of Birth: 07 November 1988, Ankara
Marital Status: Single
Phone: +90 506 770 25 39
Email: sbcelik@ybu.edu.tr

EDUCATION

Degree	Institution	Year of Graduation
B. Sc.	Çankaya Univ., Electronics and Communication Engineering	2012
High School	Etimesgut Anatolian High School	2006

WORK EXPERIENCE

Year	Place	Enrollment
2014 Sept. - Present	Yıldırım Beyazıt Univ., Department of The Electrical and Electronics Engineering	Research Assistant
2012 September -2014 September	Başkent Univ., Department of The Electrical and Electronics Engineering	Research Assistant
2010 August	Aselsan Inc.	Intern
2010 July	TRT	Intern

FOREIGN LANGUAGES
English, Beginner Italian, Beginner Spanish

HONOURS AND AWARDS

1. Master Education Full Scholarship 2012
   Çankaya University
2. Graduate High Honour Student 2012
   Çankaya University
3. Graduate Education Full Scholarship 2007
   Çankaya University
4. Football Tournament Championship 2014
   Çankaya University
5. Futsal Tournament Championship 2013
   Çankaya University
6. Football Tournament Championship 2013
   Çankaya University

HOBBIES
PC, Music, Football, Basketball, Books